Journal of FOOD PROCESSING AND PRESERVATION

Edited by T. P. Labuza, University of Minnesota

FOOD & NUTRITION PRESS, INC.
WESTPORT, CONNECTICUT 06880 USA

VOLUME 2, NUMBER 3 QUARTERLY

JOURNAL OF FOOD PROCESSING AND PRESERVATION

Editor: **T. P. LABUZA**, Department of Food Science and Nutrition, University of Minnesota, St. Paul, Minnesota

Assistant Editor: **ALLA L. PETRENKO**, Department of Food Science and Nutrition, University of Minnesota, St. Paul, Minnesota

All articles for publication and inquiries regarding publication should be sent to Prof. T. P. Labuza, University of Minnesota, Department of Food Science and Nutrition, St. Paul, Mn. 55108 USA.

All subscriptions and inquiries regarding subscriptions should be sent to Food & Nutrition Press, Inc., 265 Post Road West, Westport, Connecticut USA.

One volume of four issues will be published annually. The price for Volume 2 is $50.00 which includes postage to U.S., Canada, and Mexico. Subscriptions to other countries are $60.00 per year via surface mail, and $67.00 per year via airmail.

Subscriptions for individuals for their own personal use are $30.00 for Volume 2 which includes postage to U.S., Canada, and Mexico. Personal subscriptions to other countries are $40.00 per year via surface mail, and $47.00 per year via airmail. Subscriptions for individuals should be sent direct to the publisher and marked for personal use.

The *Journal of Food Processing and Preservation* is published quarterly by Food & Nutrition Press Inc. — Office of publication is 265 Post Road West, Westport, Connecticut 06880 USA.

Application to mail at second class postage rates is pending at Westport, Ct. 06880.

JOURNAL OF FOOD PROCESSING AND PRESERVATION

JOURNAL OF FOOD PROCESSING AND PRESERVATION

Journal of
FOOD PROCESSING AND PRESERVATION

VOLUME 2
NUMBER 3

FOOD & NUTRITION PRESS, INC.
WESTPORT, CONNECTICUT 06880 USA

ISSN: 0145-8892

Printed in the United States of America

CONTENTS

MONTE CARLO SIMULATION OF NUTRIENT BASED SERVING SIZES OF FOOD[1]

ROBERT C. WARD, JUDSON M. HARPER and NORMAN B. JANSEN

Department of Agricultural and Chemical Engineering
Colorado State University
Fort Collins, Colorado 80523

Received for Publication September 11, 1978

ABSTRACT

Monte Carlo simulation and linear programming are combined to form a procedure for evaluating the serving sizes of foods needed to meet minimum nutritional standards (RDA female and male and U.S. RDA). The procedure is described and applied using over 400 common food items to simulate hundreds of thousands of meals. Once each meal is randomly chosen via Monte Carlo simulation, linear programming is used to determine the food serving size that meets nutrient standards while at the same time minimizing the deviation from currently accepted standard serving sizes. The serving sizes are to be analyzed to compare the effect of different standards, calorie levels, and meals (breakfast, lunch and dinner). The paper describes the methodology used in the simulation and presents examples of the results obtained.

INTRODUCTION

Serving sizes of food currently have little, if any, relationship to specific nutritional requirements. The purpose of this paper is to describe a procedure (mathematical simulation) by which serving sizes of food can be related to a specific nutritional standard.

The procedure involves selecting 400 common food items and placing them into food groups with from one item up to 32 items appearing in each group. The food groups contain food items with similar characteristics. For example, the food group entitled "plain starches" contains rice, baked potato, mashed potatoes, noodles, etc. Menus are then developed using these food groups. For example, a breakfast menu might consist of four groups: fruit juice, cereal and sugar, milk for cereal and

[1] Work reported in this paper was supported by a contract with HEW/FDA #223-74-2088

beverage. A specific meal is then created by randomly selecting items from each food group. Since the items in each food group can be interchanged, it is possible to create a large number of specific meals for each general menu type being considered in the simulation.

Linear programming is used to determine the serving size of the food items which will meet the nutritional requirements. While satisfying the nutrient constraints, the linear programming algorithm minimizes the deviation from currently accepted serving sizes of all items in the meal. For each menu (43 are used) several thousand specific, randomly selected meals are examined and required serving sizes are calculated.

Statistics on the computed serving sizes for each nutrient constraint are retained. The average serving size and standard deviation are computed for each menu and overall menus, resulting in a recommended average serving size for each food item.

With this brief summary to help establish the overall strategy, each aspect of the simulation will now be examined in detail.

MENU AND NUTRIENT DATA ORGANIZATION

The menu items used in the simulation were selected from a computerized food item file at Colorado State University. The items were selected to represent a wide spectrum of foods and to reasonably represent the collection of menu items from which the United States population select their daily food intake.

Following selection of the food items to be considered, the items were divided into 41 groups. The food groups represent combinations of like items. Examples of the food groups are cereals with sugar, vegetables, sandwiches, meat entrees and beverages.

Within each group, each food item was assigned a frequency of service. This frequency was based on existing data—the main reference being the statistics published by Meiselman, Waterman and Symington (1974). The above information was combined with the currently accepted normal serving sizes (Jansen and Harper 1975) and the nutrients available per gram of the food item (Watt and Merrill 1963).

Three nutrient standards were chosen for the analysis. These standards are based on the Recommended Dietary Allowance (RDA) established by the Food and Nutrition Board (1973) for the 23–50 year old female and male and the United States Recommended Daily Allowance (USRDA) established by FDA (1973). For the RDA standards, the calorie levels were varied ±20% from the given calorie level while for the USRDA low, medium and high calorie levels of 2000, 2700, and 3400

kilocalories per day were chosen. This variation on calories was made to evaluate the impact of different calorie intakes. (In the simulation calorie level is the only "nutrient" which is an equality constraint.) With the calorie variation, a total of 9 different standards were used in the simulation (3 standards with 3 calorie levels for each). The standards are given in Table 1. During the simulation, a breakfast menu was required to supply 25% of the standard; lunch, 33%; and dinner, 42%.

The nutrient standards used in the simulation require additional interpretations for protein and niacin. The RDA's also permit the use of niacin equivalents synthesized from tryptophan in the computation of total niacin. The USRDA standard for protein is 45 g per day for proteins of quality equal to that of casein and 65 g per day for protein with a quality less than that of casein. Also the USRDA only considers niacin which exist preformed in the food. Each of these factors was taken into consideration in the simulation as noted in Table 1. For the purposes of the analysis, foods where more than 90% of the protein is of animal origin were considered to have an RDA of 45 g and all other proteins 65 g per day.

Forty-three menus (combinations of food groups) were chosen to be used in the simulation. The menus consisted of as few as 3 food groups in some breakfasts and lunches to as many as 9 groups for some dinners. Ten menus were a breakfast or brunch combination, 21 were a luncheon or supper combination, and 9 were a dinner combination.

SIMULATION OF RANDOM SELECTION OF MENU ITEMS

In the simulation a menu, with its food groups, is first established. Specific items are then randomly selected from each group to create a specific meal for further analysis. This random selection process was accomplished by placing all of the items in a group in an array of 100. The number of times an item appears in the array corresponds to its relative frequency of service. For example, if green beans appear 6% of the time when a vegetable is served, green beans will be assigned 6 positions in the vegetable array.

To select a specific food item from each group, a random number between 1 and 100 is generated, thus identifying the particular item from each group of the menu to be considered. This process is repeated from each group in the menu until all specific items for a meal have been chosen.

Following selection of the food items for a meal, the nutrient data for each item is recalled from the food file in order to establish the data needed for the linear programming optimization.

Table 1. Nutrient standards used in the simulation model[1]

	Standard[2] Number	Energy K cal	Protein g	Vitamin A I. U.	Vitamin C mg	Niacin mg	Riboflavin mg	Thiamin mg	Calcium mg	Iron mg
RDA	1	1600								
Female	2	2000	46	4000	45	13[3]	1.2	1.0	800	18
(23–50)	3	2400								
RDA	4	2160								
Male	5	2700	56	5000	45	18[3]	1.6	1.4	800	10
(23–50)	6	3240								
USRDA	7	2000								
	8	2700	45[4]	5000	60	20	1.7	1.5	1000	18
	9	3400								

[1] These standards are based on the 1973 revised RDA's of the Food and Nutrition Board, NAS-NRC
[2] For future reference in the Results Section of the paper
[3] Niacin contribution from tryptophan was adjusted by 0.1667 × protein
[4] Protein contribution of all foods with <90% animal protein was adjusted by the factor 45/65

OPTIMIZATION OF SERVING SIZES

The linear programming formulation, used to determine the serving size of the food item which satisfies the nutrient standards and minimizes deviation from the normal serving size now used, can be stated as follows:

$$\text{Min } z = \sum_{i=1}^{n} (E_i + F_i) \tag{1}$$

subject to

$$\frac{X_i}{C_i} + E_i - F_i = 1, \qquad i = 1, 2, \ldots, n \tag{2}$$

$$\sum_{i=1}^{n} A_{ij} X_i \; (\geqslant, =) \; b_j \qquad j = 1, 2, \ldots, m \tag{3}$$

where n is the number of items in the meal and m is the number of nutrients in the standard being considered. The normal serving size currently used is C_i, the nutrients available per gram of the food item is A_{ij}, the nutrient standard is b_j and the new serving size (the decision variable) is X_i. Letters E_i and F_i are employed to have the linear program determine the serving sizes which not only meet the nutrient standards, but which also provide the smallest change from the normal serving size currently used. Two variables are needed to permit the change to be either positive or negative (Equation 2). By minimizing both the positive or negative deviations from the C_i (Equation 1), the linear programming solution ensures that the nutrient standards are met (Equation 3) with minimum percentage change in the serving size of any one item. In Equation 3, the signs in parentheses indicate that all of the nutrients are greater-than-or-equal-to the type of constraints except for calories which is an equality constraint.

The constraints expressed in Equation 2 imply that the linear programming solution will minimize percentage changes in the serving sizes of food. If Equation 2 had been expressed as follows:

$$C_i - X_i + E_i - F_i = 0, \qquad i = 1, 2, \ldots, n, \tag{4}$$

the absolute differences in the serving sizes would have been minimized. Equation 4 was not chosen for the linear programming formulation

because the chance of having serving sizes of items go to zero is greater than if Equation 2 is used. Such a condition was felt to be unsatisfactory for it would remove entire items from the meal and would not give a reasonable value for a serving size based on nutrients.

PROBLEM SOLUTION

The computerized food file, the random selection of specific meals and the linear programming optimization of serving sizes are combined into one computer program. A flow chart illustrating the overall strategy of the simulation is shown in Fig. 1. Due to the size of the simulation, it was broken down into several separate computer programs. However, for purposes of discussion, the simulation will be described as one program, as shown in Fig. 1.

In the simulation program, the menu (combination of food groups) to be analyzed is read into the computer, along with data that identifies the menu as a breakfast, lunch or dinner. Next the food items, which are to constitute a specific meal, are randomly chosen. The food file is then entered and the A_{ij} and C_j for the linear programming formulation are quantified. The b_i are determined based on whether the menu is a breakfast, lunch or dinner. The linear programming algorithm (revised simplex) then determines the optimum serving size under the given constraints. The computed serving sizes are then stored. If all 9 standards (3 standards with 3 calorie levels for each) have been analyzed, control then goes back to select another specific meal for the menu being considered and the process is repeated. After all the meals have been analyzed for this menu, another menu is read and the process repeated.

For each menu, the statistics retained are: (1) the total number of times an item appeared in the meals; (2) the number of times an item appeared in feasible solutions; (3) the sum of serving sizes for each item; and (4) the sum of the squares of the serving sizes for each item. The latter 3 statistics were not only stored for each item, but also for each of the 9 standards. The first statistic was common across the nine standards.

For each menu, the average and standard deviation of the serving size of each item for each standard was computed. The mean and standard deviation was also computed across each standard, across low, medium and high calorie levels, and across all standards (or calorie levels) for a final total. The above statistics were also computed across all breakfast menus, lunch menus and dinner menus, and across all the menus. In all

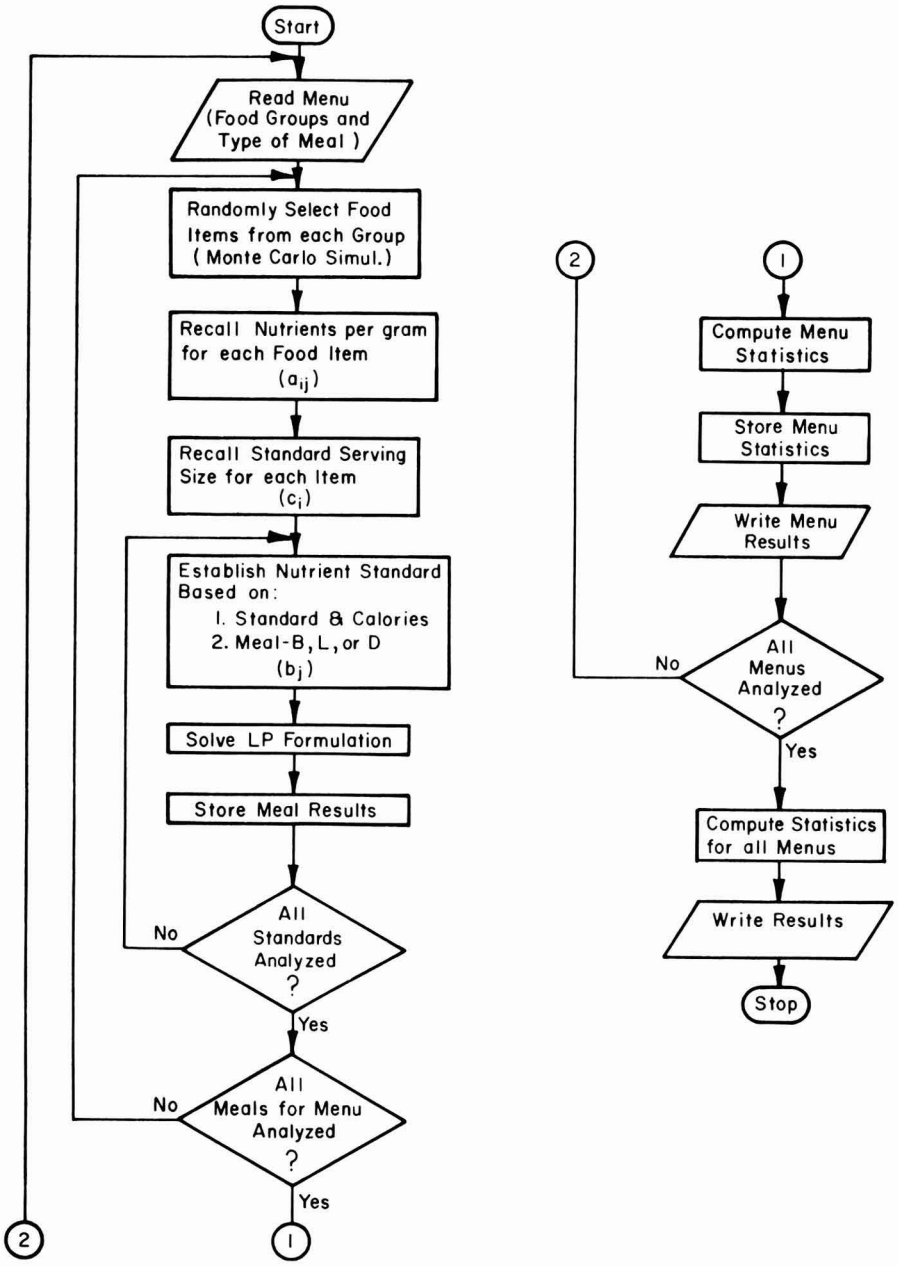

FIG. 1. FLOW CHART OF SERVING SIZE SIMULATION

cases, the total number of times an item appeared and the number of times it appeared in feasible solutions was noted.

The number of specific meals analyzed for any one menu depended upon the number of feasible solutions obtained. In certain combinations, especially with the 3 and 4 food group menus, the nutrient to calorie ratio of the foods was not large enough to meet the minimum nutrient constraints *and* satisfy the calorie equality constraint. This resulted in infeasible solutions in the linear programming algorithm (i.e. no feasible combinations could meet the nutrient standards while satisfying the calorie constraint).

For a given menu, enough meals were analyzed so that the food item with the lowest frequency appeared in at least 20 feasible solutions. An evaluation of feasible versus infeasible solutions revealed that, for 5 item menus and above, the program averaged approximately 70% feasible solutions. Since 1% was the smallest frequency of serving permitted, the number of meals needed to be analyzed was 2857 (rounded to 3000 in the program). For a higher rate of infeasible solutions, the number of meals analyzed would have to be increased.

The simulation program was run on the Colorado State University CDC 6400. Menus with 5 items or more averaged approximately 2.3 s of central processor time per meal (over all standards). This resulted in an average time of 1.9 h per menu (for 3000 meals). Menus with less food groups averaged less time per meal, but required more meals to be analyzed due to the infeasible solutions.

RESULTS

While preparing the simulation program for "production" runs, several smaller tests were made to ensure that the program was performing as designed. In these smaller tests, which did indicate proper performance, considerable detail was printed out on each meal. From this detail, it is possible to get a better feel for what is happening inside the program. Table 2 contains the results of 6 meals—3 from a 4 item breakfast menu and 3 from a 6 item dinner menu. Each menu contained the following food groups:

Breakfast	Dinner	
Fruit juice	Meat entree	Vegetable
Cereal and sugar	Starch-plain	Butter for vegetable
Milk for cereal	Gravy for meat and starch	Beverage
Beverage		

Table 2 gives a rough idea of the meals being generated, the number of infeasible solutions, the nutrients causing infeasibility and the serving sizes being generated within specific meals. Forcing the calorie constraint to be an equality created many of the anomolies in the table. The nutrients simply could not be obtained from the meal without violating the calorie constraint.

Following testing phase, production runs were made. Except for the 3 and 4 item menus, 3000 meals were generated and analyzed for each menu. The mean serving sizes, standard deviation and number of feasible solutions were computed and printed for each menu. The results from one menu represent serving sizes of food needed to meet nutrition standards when only food items from the food groups in that menu are permitted in the meal. Consequently, for any one menu, serving sizes for any particular item may be very large or small, depending upon the menu. This menu effect is damped when all menu results are combined.

In Table 3 the results of one menu are presented. The menu is the dinner menu listed above. One item from each food group was selected to be included in the table. Since butter is the only food item in its group, it appeared 3000 times. The serving frequency and number of appearances are listed for each item. The totals represent the total appearances and average serving sizes over the corresponding row or column. For this menu, vegetables tended to be very large (cabbage, shown in the table, was one of the largest), when compared to the current serving size. Coffee also was very large due to the calcium and niacin available with almost no calories.

Once all of the menus were analyzed, totals for all breakfast menus were computed as were all lunch menus and all dinner menus. (Eventually, a total sum for each food item overall menus is desired to give a general indication of what the average serving size for that food should be if it is to meet nutrient standards.) In Table 4, the results of 6 of the food items involved in the breakfast menus are presented. In this table the total number of appearances depends not only upon the serving frequency, but also on the number of times the food group was included in the 10 menus. For example, eggs in Table 4 belong to the non-meat entrees food group which appears in 3 breakfast menus, while brunch meats, which bacon belongs to, was included in 4 menus.

The serving sizes in Table 4 do not contain the wide fluctuations of the previous tables. As more menus are combined, a dampening effect on the extreme sizes occurred. For example, although not in Table 4, black coffee for all breakfast menus, had a final mean serving size of 631 g.

Table 2. Example of simulation results for specific meals

Meal	Currently Accepted Normal Serving Size (grams)	Nutrient Standards[1]								
		1	2	3	4	5	6	7	8	9
		Computed Serving Sizes (grams)								
Breakfast										
1. Dry fruit and nuts breakfast cereal	28	Vitamin A[2]					17	Vitamin A		
Whole milk	244	Vitamin C	Vitamin C	Iron	Vitamin A	Vitamin C	863	Vitamin C	Vitamin A	Vitamin C
Grape juice	186	Thiamin	Iron		Vitamin C		186	Thiamin	Vitamin C	
Coffee with milk and sugar	283	Iron					283	Iron		
2. Corn grits, cooked	185	Vitamin A		185	Vitamin A	185	185	Vitamin A		850
Whole milk	244	Vitamin C	Iron	569	Vitamin C	774	617	Vitamin C	Thiamin	463
Pineapple juice	186	Thiamin		186	Thiamin	113	569	Thiamin	Iron	186
Black coffee	240	Iron		3391	Iron	1609	240	Iron		1395
3. Ready to eat cereal	28	28	28	28	28	28	28	28	28	28
Whole milk	244	391	545	699	607	815	1023	545	815	1084
Tomato juice	181	181	181	181	181	181	181	181	181	181
Black coffee	240	240	240	240	240	240	240	240	240	240

[1] Numbers on standards refer to numbering used in Table 1
[2] Where nutrient list replaces serving size, an infeasible solution occurs and listed nutrients are ones that were not met

(Continued)

Table 2. Example of simulation results for specific meals (continued)

Meal	Currently Accepted Normal Serving Size (grams)	Nutrient Standards[1]								
		1	2	3	4	5	6	7	8	9
		Computed Serving Sizes (grams)								
Dinner										
1. Broiled chicken	85	0	0	118	4	85	85	0	82	85
Cornbread stuffing	127	37	327	365	127	475	615	35	414	639
Cream gravy	76	76	63	76	250	76	76	76	139	76
Bean sprouts	62	489	505	245	336	194	160	735	307	259
Butter	10	42	10	10	41	10	10	54	10	10
Black coffee	240	8244	240	240	240	240	240	10307	240	240
2. Lamb chops	90	21	61	111	93	159	225	29	117	204
Baked potatoes	100	100	100	100	100	100	100	100	100	100
Cream gravy	76	194	210	221	236	227	219	298	318	338
Squash	105	306	276	277	392	394	396	365	366	368
Butter	10	7	10	10	10	10	10	10	10	10
Coffee with milk and sugar	283	705	645	550	283	283	283	630	464	299
3. Spareribs	85	77	85	131	24	49	100		98	136
Cornbread stuffing	127	0	123	127	355	367	367		281	365
Brown gravy	77	0	0	46	0	77	77	Riboflavin	77	77
Cabbage	73	1857	1457	1014	227	73	73	Iron	364	306
Butter	10	0	0	0	10	10	10		0	10
Whole milk	244	0	0	0	142	244	244		24	48

[1] Numbers on standards refer to numbering used in Table 1

[2] Where nutrient list replaces serving size, an infeasible solution occurs and listed nutrients are ones that were not met

Table 3. Example results from a dinner menu[1]

	Food Item	Current Serving Size	Serving Frequency	Total Number of Appearances	Number of Feasible Solutions	Mean Serving Size	Standard Deviation	Number of Feasible Solutions	Mean Serving Size	Standard Deviation	Number of Feasible Solutions	Mean Serving Size	Standard Deviation	Number of Feasible Solutions	Mean Serving Size	Standard Deviation
					672 kcal			840 kcal			1008 kcal			Total		
RDA Female (23–50)	Broiled chicken	85	4	123	86	109	92	107	145	108	112	187	128	305	150	116
	Cornbread stuffing	127	12	351	264	116	73	303	183	91	331	265	112	898	194	112
	Brown gravy	77	55	1667	1178	55	38	1368	63	36	1522	70	31	4068	63	35
	Cabbage	73	3	90	90	1165	454	90	773	386	90	490	340	270	809	482
	Butter	10	100	3000	2220	8	9	2556	10	9	2779	11	8	7555	10	9
	Black coffee	240	22	631	549	1638	2767	607	1311	2832	629	1029	2507	1785	1312	2711
					907 kcal			1134 kcal			1360 kcal			Total		
RDA Male (23–50)	Broiled chicken	85	4	123	107	96	76	117	153	133	121	225	212	345	160	162
	Cornbread stuffing	127	12	351	312	262	100	345	373	106	351	429	139	1008	358	135
	Brown gravy	77	55	1667	1395	65	35	1549	75	41	1606	78	52	4550	73	44
	Cabbage	73	3	90	90	712	466	90	286	347	90	185	227	270	394	425
	Butter	10	100	3000	2606	13	11	2875	14	11	2939	13	10	8420	13	11
	Black coffee	240	22	631	562	593	1682	619	736	2276	629	613	1962	1810	649	1997

[1] 3000 meals were analyzed to obtain these results

(Continued)

Table 3. Example results from a dinner menu[1] (continued)

	Food Item	Current Serving Size	Serving Frequency	Total Number of Appearances	Number of Feasible Solutions	Mean Serving Size	Standard Deviation	Number of Feasible Solutions	Mean Serving Size	Standard Deviation	Number of Feasible Solutions	Mean Serving Size	Standard Deviation	Number of Feasible Solutions	Mean Serving Size	Standard Deviation
					840 kcal			1134 kcal			1428 kcal			Total		
U.S. RDA	Broiled chicken	85	4	123	85	107	82	109	163	125	117	241	202	305	177	158
	Cornbread stuffing	127	12	351	263	159	91	315	334	132	347	483	149	898	340	183
	Brown gravy	77	55	1667	1156	56	35	1448	67	39	1556	77	47	4068	68	42
	Cabbage	73	3	90	72	1365	534	90	637	432	90	318	296	270	731	598
	Butter	10	100	3000	2156	9	10	2690	12	11	2870	12	9	7555	11	10
	Black coffee	240	22	631	502	1451	2889	606	1248	3502	629	895	2809	1785	1179	3097
					Low kcal			Medium kcal			High kcal			Total		
Total	Broiled chicken	85	4	369	278	103	83	333	153	123	350	218	186	961	163	148
	Cornbread stuffing	127	12	1053	839	184	109	963	300	137	1029	395	163	2831	300	164
	Brown gravy	77	55	5001	3729	59	36	4365	69	39	4684	75	43	12778	68	41
	Cabbage	73	3	270	252	1060	552	270	566	439	270	331	316	792	643	536
	Butter	10	100	9000	6982	10	11	8121	12	10	8588	12	9	23691	12	10
	Black coffee	240	22	1893	1613	1215	2529	1832	1096	2919	1887	846	2456	5332	1043	2649

[1] 3000 meals were analyzed to obtain these results

Table 4. Example results from combination of all breakfast menus

	Food Item	Current Serving Size	Serving Frequency	Total Number of Appearances	Number of Feasible Solutions	Mean Serving Size	Standard Deviation	Number of Feasible Solutions	Mean Serving Size	Standard Deviation	Number of Feasible Solutions	Mean Serving Size	Standard Deviation	Number of Feasible Solutions	Mean Serving Size	Standard Deviation
					400 kcal			500 kcal			600 kcal			Total		
RDA Female (23–50)	Eggs, scrambled or fried	65	34	2998	844	109	48	1971	159	57	2417	148	52	5232	146	56
	Bacon, broiled or fried	30	32	5072	1057	4	9	1546	8	11	2255	12	12	4858	9	11
	Ready-to-eat cereal	28	27	5200	5200	29	5	5200	30	8	5200	31	12	15600	30	9
	Bananas, raw	119	6	795	215	113	20	468	164	101	692	201	149	1375	175	125
	Grapefruit juice, unsweetened	186	12	2827	544	148	70	839	141	68	1212	141	71	2595	143	70
	Whole milk	244	10	3303	1159	76	74	1557	121	104	2011	160	129	4727	126	114
					540 kcal			675 kcal			810 kcal			Total		
RDA Male (23–50)	Eggs, scrambled or fried	65	34	2998	2076	128	56	2476	124	56	2749	119	64	7301	123	59
	Bacon, broiled or fried	30	32	5072	1689	13	13	2460	18	14	2876	27	15	7025	20	15
	Ready-to-eat cereal	28	27	5200	5200	30	10	5200	31	15	5200	31	21	15600	31	16
	Bananas, raw	119	6	795	368	117	5	787	170	119	795	153	104	1950	153	102
	Grapefruit juice, unsweetened	186	12	2827	837	172	45	1369	162	61	1605	177	33	3811	171	48
	Whole milk	244	10	3303	1961	195	91	2380	270	113	2952	353	190	7293	283	158

(Continued)

Table 4. Example results from combination of all breakfast menus (continued)

	Food Item	Current Serving Size	Serving Frequency	Total Number of Appearances	Number of Feasible Solutions	Mean Serving Size	Standard Deviation	Number of Feasible Solutions	Mean Serving Size	Standard Deviation	Number of Feasible Solutions	Mean Serving Size	Standard Deviation	Number of Feasible Solutions	Mean Serving Size	Standard Deviation
					500 kcal			675 kcal			850 kcal			Total		
U.S. RDA	Eggs, scrambled or fried	65	34	2998	629	112	61	1523	120	72	2147	125	71	4299	121	70
	Bacon, broiled or fried	30	32	5072	822	8	11	1328	19	16	2292	30	23	4442	23	21
	Ready-to-eat cereal	28	27	5200	5200	30	8	5200	31	15	5200	32	22	15600	31	16
	Bananas, raw	119	6	795	154	122	10	548	293	207	753	298	201	1455	277	200
	Grapefruit juice, unsweetened	186	12	2827	440	168	48	757	158	59	1202	161	53	2399	161	54
	Whole milk	244	10	3303	1044	137	99	1435	205	127	2019	242	169	4498	206	148
					Low kcal			Medium kcal			High kcal			Total		
Total	Eggs, scrambled or fried	65	34	8994	3549	121	56	5970	135	63	7313	130	64	16832	130	62
	Bacon, broiled or fried	30	32	15216	3568	9	12	5334	15	14	7423	23	19	16325	18	17
	Ready-to-eat cereal	28	27	15600	15600	30	8	15600	30	13	15600	31	19	46800	30	14
	Bananas, raw	119	6	2385	737	117	13	1803	206	158	2240	216	167	4780	197	154
	Grapefruit juice, unsweetened	186	12	8481	1821	164	55	2965	155	63	4019	161	55	8805	160	58
	Whole milk	244	10	9909	4164	147	102	5372	209	130	6982	265	187	16518	217	159

The results of summing over all menus for 7 typical foods used mainly in dinner menus are given in Table 5. These data show very large serving size requirements for green beans and lettuce which supply high levels of nutrients with the addition of few calories. The serving sizes for these items are unrealistically large and a constraint on bulk and fiber would have to be imposed to develop more appropriate serving sizes.

The reduced serving size on the vinegar and oil dressing and wine are examples where the program reduced serving sizes because these items contributed little but calories. The reduction in serving size of these items was most evident for menus with a low calorie constraint.

DISCUSSION

The averaged results of the simulation indicate what the average serving sizes of foods should be if minimum nutritional standards are to be met. Most of the computed serving sizes deviated from the currently accepted normal serving sizes by reasonable amounts. Most of the deviations can readily be explained—items high in nutrients and low in calories generally show an increase in serving size while items low in nutrients and high in calories generally show a decrease in serving size. This is not the situation in all cases as some deviations were the result of some complex and rather subtle characteristics of the foods and the simulation.

Results which were surprising can best be discussed by first recalling some of the more basic assumptions made in the simulation. The assumptions to be discussed are summarized below.

1. Nutritional standards are required to be met with common food items combined in commonly accepted menus
2. Nutritional standards must be met at each meal in proportion to that meal's contribution (25% for breakfast, 33% for lunch, and 42% for dinner)
3. The calorie constraint is an equality—it had to be met exactly for each meal
4. Serving sizes are optimized in such a way that minimum deviation from the currently accepted size occurs as the nutritional standards are being met

Since the food items and menu combinations used in the simulation are quite common to the United States diet (assumption one), a computed serving size that deviates greatly from the currently accepted

Table 5. Example results from combination of all menus, illustrating mainly dinner food items

	Food Item	Current Serving Size	Serving Frequency	Total Number of Appearances	Number of Possible Solutions	Mean Serving Size	Standard Deviation	Number of Possible Solutions	Mean Serving Size	Standard Deviation	Number of Possible Solutions	Mean Serving Size	Standard Deviation	Number of Possible Solutions	Mean Serving Size	Standard Deviation
					400 kcal			500 kcal			600 kcal			Total		
RDA Female (23–50)	Spaghetti with meat sauce	222	6	895	787	380	86.2	893	376	70.0	893	399	91.2	2573	385	83.4
	Beans, green, canned	71	6	2464	2293	342	181.8	2351	278	165.7	2372	233	156.8	7017	284	174.1
	Lettuce wedge	41	17	4113	4110	401	295.4	4106	292	260.2	4105	226	224.0	12321	306	271.0
	Vinegar & oil dressing	14	19	4425	2575	1	3.7	2980	4	6.0	3281	7	6.6	8836	4	6.2
	French bread	50	9	2673	1330	35	29.8	1684	46	37.9	1949	58	45.6	4963	48	40.4
	Butter	10	100	56995	36230	5	6.0	42752	7	6.1	47460	9	5.4	126442	7	6.0
	Wine, table	116	1	1471	548	56	52.9	685	80	49.9	843	94	41.4	2076	79	49.9
					540 kcal			675 kcal			810 kcal			Total		
RDA Male (23–50)	Spaghetti with meat sauce	222	6	895	873	410	114.9	879	461	121.1	878	563	187.3	2630	478	158.3
	Beans, green, canned	71	6	2464	2192	330	279.9	2229	232	220.4	2282	185	188.4	6703	248	239.7
	Lettuce wedge	41	17	4113	4075	250	233.6	4074	192	202.5	4072	156	174.4	12221	199	208.6
	Vinegar & oil dressing	14	19	4425	2911	7	6.5	3436	10	5.6	3811	12	4.5	10158	10	6.0
	French bread	50	9	2673	1808	51	26.4	2130	58	30.0	2304	66	43.5	6242	59	35.3
	Butter	10	100	56995	43756	9	6.7	48863	11	6.5	51887	11	6.3	144506	10	6.6
	Wine, table	116	1	1471	757	61	53.7	906	92	44.3	1040	106	33.7	2703	89	47.3

(Continued)

Table 5. Example results from combination of all menus, illustrating mainly dinner food items (continued)

	Food Item	Current Serving Size	Serving Frequency	Total Number of Appearances	Number of Possible Solutions	Mean Serving Size	Standard Deviation	Number of Possible Solutions	Mean Serving Size	Standard Deviation	Number of Possible Solutions	Mean Serving Size	Standard Deviation	Number of Possible Solutions	Mean Serving Size	Standard Deviation
					500 kcal			675 kcal			850 kcal			Total		
U.S. RDA	Spaghetti with meat sauce	222	6	895	694	442	121.9	894	501	106.5	895	614	183.8	2483	526	159.3
	Beans, green canned	71	6	2664	2137	596	421.3	2258	346	292.6	2331	250	240.0	6726	392	355.0
	Lettuce wedge	41	17	4113	4107	499	361.5	4098	299	295.5	4102	222	246.9	12307	340	326.6
	Vinegar & oil dressing	14	19	4425	2464	4	7.2	3028	8	7.1	3608	12	5.8	9100	9	7.2
	French bread	50	9	2673	1229	48	35.3	1725	71	46.4	2094	84	55.5	5048	71	50.1
	Butter	10	100	56995	33631	7	6.8	43882	9	6.3	49336	11	5.8	126849	9	6.5
	Wine, table	116	1	1471	522	52	54.0	711	82	49.6	895	103	35.5	2128	83	49.7
					Low kcal			Medium kcal			High kcal			Total		
Total	Spaghetti with meat sauce	222	6	2685	2354	409	111.2	2666	446	114.1	2666	525	184.7	7686	462	149.9
	Beans, green, canned	71	6	7392	6622	420	330.8	6838	285	236.0	6986	223	199.7	20446	308	272.8
	Lettuce wedge	41	17	12339	12292	384	318.4	12278	261	260.3	12279	201	219.7	36849	282	279.6
	Vinegar & oil dressing	14	19	13275	7950	4	6.4	9444	8	6.8	10700	10	6.1	28094	8	6.9
	French bread	50	9	8019	4367	45	30.9	5539	58	39.3	6347	69	49.5	16253	59	42.8
	Butter	10	100	170985	113617	7	6.7	135497	9	6.5	148683	10	6.0	397797	9	6.5
	Wine, table	116	1	4413	1827	57	53.6	2302	85	48.0	2278	101	37.1	6907	84	49.0

serving size indicated the item is being used to meet a possible deficiency in the diet (a deficiency as defined by the nutritional standard being met). If the serving size deviation is on the large side, vitamins and minerals may need to be supplemented if that particular item is to be eaten in less quantities than computed. The large serving size situation, as expected, is most prevalent in the low calorie standards.

Requiring each meal to meet a specific nutritional level (assumption two) does not permit one meal to be below standard, while another meal, that same day, is above standard, thus meeting the daily nutrient level. This fact explains why some items are extremely large for a dinner menu, but are reduced for a breakfast menu. Coffee is an example of these items. Calcium was not as available in the dinner food items as it was in the breakfast items, thus coffee was called on to supply the calcium, mainly because it contributed the nutrient with very few calories.

Assumption three also explains why some items developed large deviations. The nutrients had to be supplied without violating the calorie constraint; consequently, those items with many nutrients and few calories were increased in size (some very large). A review of the serving sizes as the calorie constraint is loosened (made larger) reveals that the extremely large serving sizes tend to get smaller as the calories are permitted to increase. Likewise, items low in nutrients and high in calories may have extremely small serving sizes in low calorie meals, but as the calorie constraint is loosened, the serving size is increased. Items low in nutrients and high in calories tended to be in non-feasible solutions much more often than more balanced foods.

Assumption four tended to keep the serving sizes as close to that now accepted as the nutrient standards would permit. Consequently, when a food item developed a large deviation, it did so against the "will" or "goal" of the simulation and was only permitted in order to ensure that the standards were met.

SUMMARY AND CONCLUSIONS

A Monte Carlo simulation model has been described which determines food serving sizes needed to meet minimum nutritional standards (RDA female and male and U.S. RDA). The model uses over 400 common food items to simulate hundreds of thousands of meals. Once each meal is randomly chosen, linear programming is used to determine the food serving size that meets nutrient standards while at the same time minimizing the deviation from currently accepted standard serving

sizes. The serving sizes are analyzed to compare the effect of different standards, calorie levels, and meals (breakfast, lunch and dinner).

The simulation performed satisfactorily, producing results that are potentially useful in relating serving sizes of food to nutritional standards. Most of the computed serving sizes are within a reasonable deviation from the currently accepted serving size. Nutritional implications of the findings will be discussed in a subsequent publication.

ACKNOWLEDGMENTS

The authors are grateful for the assistance of C. T. Shigetomi in preparing this and for the financial and technical support of the Food and Drug Administration (Contract 74-88, Mary Ann Stevan, Project Officer).

REFERENCES

Food and Drug Administration. 1973. Food Labeling. Federal Register 38(13): 2124 (part II) and 38(4): 6950 (part I).

Food and Nutrition Board. 1973. Recommended Dietary Allowances, Eighth Revised Edition, National Academy of Sciences, Washington, D.C.

JANSEN, F. R., and HARPER, J. M. 1975. Consumer Food and Menu Planner, Departments of Food Science and Nutrition and Agricultural Engineering, Colorado State University, prepared for the Food and Drug Administration, February.

MEISELMAN, H. L., WATERMAN, D. and SYMINGTON, L. E. 1974. Armed Forces Food Preferences, Technical Report 75-63-FSL, USA Natick Development Center, Natick, MA 01760.

WATT, B. K. and MERRILL, A. L. 1963. Composition of Foods—Raw, Processed, Prepared, Revised Edition, Agricultural Handbook Number 8, USDA, Washington, D.C.

EXTENT OF NONENZYMATIC BROWNING IN GRAPEFRUIT JUICE DURING THERMAL AND CONCENTRATION PROCESSES: KINETICS AND PREDICTION

I. SAGUY, I. J. KOPELMAN and S. MIZRAHI

Department of Food Engineering and Biotechnology
Technion
Haifa, Israel

Received for Publication November 16, 1978

ABSTRACT

The kinetics of browning in grapefruit juice during thermal and concentration processes was studied. The reaction is seen to be initially slow (lag period) and later relatively rapid (post-lag period), represented by an exponential and a linear time function respectively. The effect of temperature on the rate of reaction obeys the Arrhenius equation. The activation energy, for a solids content of 11 *to* 62°*Bx, ranges from* 8 *to* 30 *Kcal/mole in the lag period and from* 15 *to* 24 *Kcal/mole in the post-lag period.*

Curve-fitting techniques yielded an empirical kinetic equation correlating the rate of reaction with temperature and degree of concentration; this equation in turn yielded a mathematical prediction model, used to advantage in studying the extent of browning in grapefruit juice during commercial thermal and concentration processes.

INTRODUCTION

Nonenzymatic browning is a major factor in quality and acceptability of citrus products, and its role is especially significant in products with a yellowish color tone, such as grapefruit and lemon concentrates. In these circumstances, proper selection of process parameters, equipment and storage conditions, with a view to minimizing the reaction, is of prime economic importance.

Since available literature on nonenzymatic browning of citrus and related products (as reviewed by Reynolds 1965; Eskin *et al.* 1971; Berk 1976) contains scanty kinetic data, the present investigation was undertaken with a view to: (1) determine the kinetics of the browning reaction in grapefruit juice and concentrate, as governed by processing conditions; (2) develop a mathematical model for prediction of the extent of browning during commercial processing.

Journal of Food Processing and Preservation 2 (1978) 175–184.

EXPERIMENTAL

Commercial grapefruit juice (Milos Citrus and Fruit Products Ltd., Nahariya near Haifa, pH 3.05; acidity as anhydrous citric acid 1.65%; solids 11.8°Bx) was tested immediately after pasteurization and cooling. The juice was concentrated to different levels in a freeze drier according to the procedure outlined by the authors in an earlier publication (1978). The concentrates were subjected to heat treatment, using the same unit and procedure. Browning measurements were carried out on diluted samples (10.0°Bx) as described by Meydav *et al.* (1977).

RESULTS AND DISCUSSION

Kinetics

Lag Period. The effect of time on the extent of nonenzymatic browning (in terms of optical density at 420 nm) in grapefruit juice concentrate is given in Fig. 1 through 3. The reaction is seen to be initially slow (lag period, t_{lag}), and later relatively rapid (post-lag period). The initial effect, observed also by Karel and Nickerson (1964), refers to the time during which colorless intermediates of the browning reaction are formed (Clegg and Morton 1965).

Curve-fitting shows the browning curves in the lag period to be exponential rather than linear:

$$B = B_o \exp(+k_L t) \quad (1)$$

where:

B = extent of browning
B_o = initial browning
k_L = constant (min^{-1})

The values of k_L, determined from Fig. 1 through 3, are listed in Table 1. The effect of temperature on k_L was calculated for each level of solids content according to the Arrhenius model, namely:

$$k_L = K_L \exp(-E_{aL}/RT) \quad (2)$$

where:

E_{aL} = activation energy
R = gas constant
K_L = constant

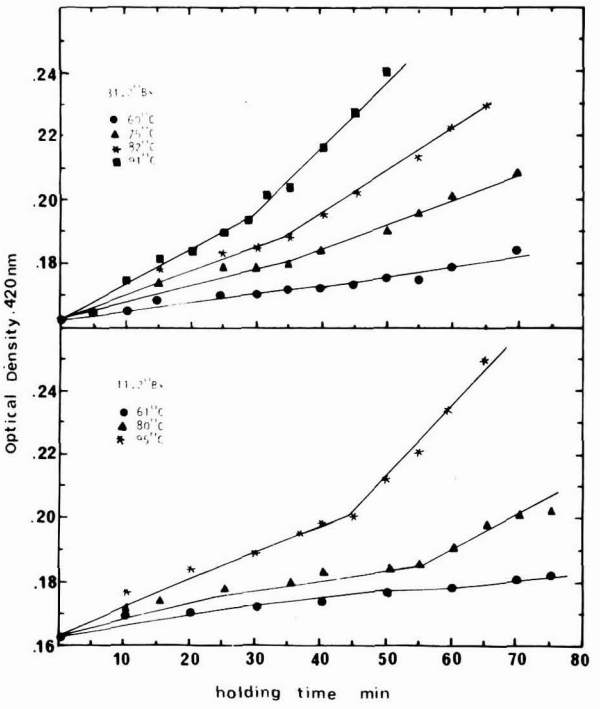

FIG. 1. EFFECT OF TIME ON BROWNING, WITH TEMPERATURE AND SOLIDS CONTENT AS CONSTANT PARAMETERS (11.2 AND 31.2°Bx)

The calculated values of E_{aL} and K_L, listed in Table 1, were further correlated with solids content, yielding the following expressions:

$$E_{aL} = 5.88 + 3.26\ (Bx/10) - 1.38\ (Bx/10)^2 + 0.24\ (Bx/10)^3 \quad (3)$$

$$K_L = \exp\ (1.506\ E_{aL} - 6.423) \qquad (r = 0.999) \quad (4)$$

The lag period as per Fig. 1 through 3 is seen to be linear with temperature at constant solids content (Fig. 4):

$$t_{lag} = t_o - b\ T \quad (5)$$

where:

T = temperature (°C)

b, t_o = constants (min/°C and min, resp)

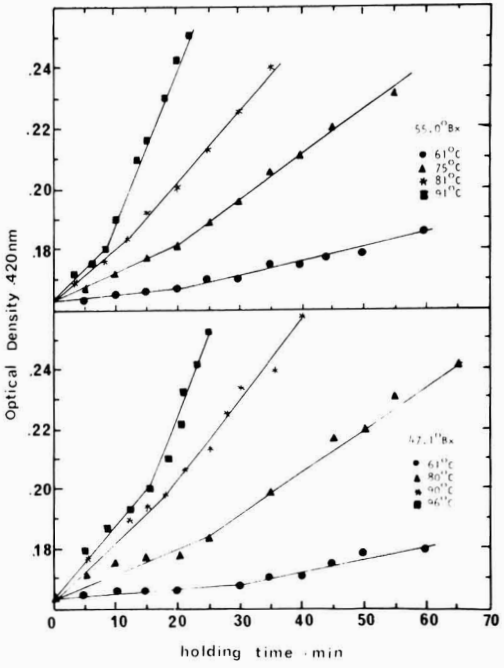

FIG. 2. EFFECT OF TIME ON BROWNING, WITH TEMPERATURE AND SOLIDS CONTENT AS CONSTANT PARAMETERS (47.1 AND 55°Bx)

Regression analysis yielded the values of b and t_o for each solids-content level (Table 2): these were subsequently found to correlate linearly with the latter, in the following form:

$$b = -2.68 + 3.26\ X_w \qquad (r = -0.983) \qquad (6)$$

$$t_o = 111.4 - 1.2\ Bx \qquad (r = -0.992) \qquad (7)$$

where:

X_w = calculated mole fraction of water

Substituting the above in Equation 5, we have:

$$t_{lag} = (111.4 - 1.2\ Bx) + (2.68 - 3.26\ X_w)\ T \qquad (8)$$

Post-lag Period. Browning in the post-lag period is linear, apparently a zero-order reaction, namely:

$$B = B_{LM} + k\,(t - t_{lag}) \tag{9}$$

where:

B_{LM} = extent of browning at end of lag period
k = constant

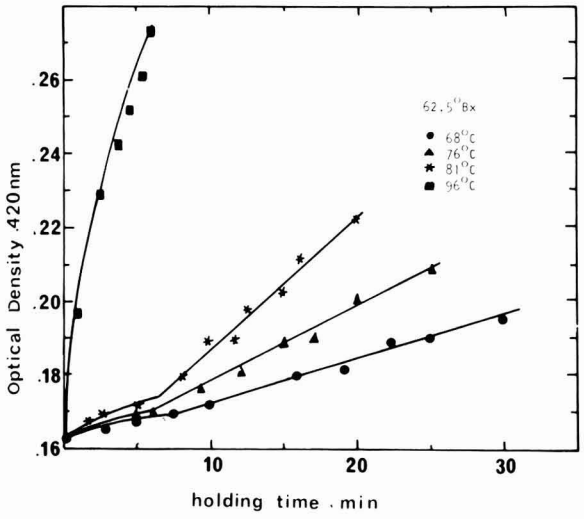

FIG. 3. EFFECT OF TIME ON BROWNING, WITH TEMPERATURE AND SOLIDS CONTENT AS CONSTANT PARAMETERS (62.5°Bx)

Applying a curve-fitting procedure in analogy to the lag period, the effects of concentration and of temperature on the reaction parameters (Table 3) are given below:

$$E_a = 14.44 + 1.28\,(Bx/10) - 0.71\,(Bx/10)^2 + 0.12\,(Bx/10)^3 \tag{10}$$

$$K_o = \exp\,(1.522\,E_a - 8.627) \qquad (r = 0.999) \tag{11}$$

where:

E_a and K_o replace E_{aL} and K_L respectively in the Arrhenius model (Equation 2).

In both periods the extent of browning increases with solids content, with a steep change upward at concentrations above 50°Bx. A similar trend was observed with regard to the effect of solids content on the rate of ascorbic acid deterioration in grapefruit concentrate (Saguy *et al.* 1978).

Table 1. Effect of temperature and solids content on the rate, Arrhenius coefficients and Q_{10} of browning formation during the lag period (k_L expressed as min^{-1})

Solids Content (°Bx)	Temperature (°C)	$k_L \times 10^3$ (min^{-1})	−r	Arrhenius Coefficients E_{aL} (kcal/mole)	ln (K_L)	−r	Q_{10} 70–80°C
11.2	61.0	1.446	0.964	8.14	5.750	0.997	1.40
	80.0	3.023	0.975				
	95.0	4.451	0.977				
31.2	60.0	1.770	0.959	9.86	8.565	0.999	1.51
	75.0	3.412	0.985				
	82.0	4.430	0.991				
	91.0	6.320	0.994				
47.1	60.0	1.461	0.986	15.50	16.831	0.995	1.90
	80.0	4.498	0.958				
	90.0	10.531	0.992				
	96.0	13.108	0.972				
55.0	61.0	1.590	0.987	21.63	26.149	0.999	2.46
	75.0	5.910	0.989				
	81.0	10.023	0.992				
	91.0	23.342	0.989				
62.5	68.0	6.055	0.992	30.41	39.387	0.962	3.54
	76.0	9.083	0.981				
	81.0	13.257	0.981				
	96.0	164.256	0.992				

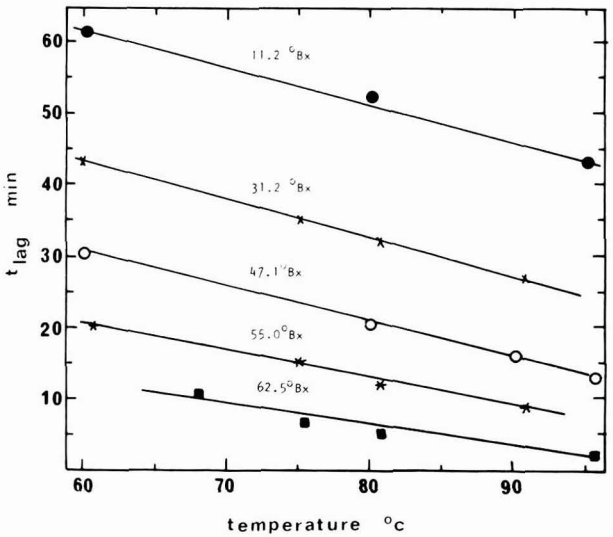

FIG. 4. EFFECT OF TEMPERATURE ON t_{lag}, WITH SOLIDS CONTENT AS CONSTANT PARAMETER

Table 2. Effect of solids content and temperature on lag time (t_{lag})

Solids Content (°Bx)	Temperature T (°C)	t_{lag} (min)	Regression Line $t_{lag} = t_o - bT$		
			t_o (min)	b (min/°C)	−r
11.2	61.0	62	96.3	0.555	0.995
	80.0	53			
	95.0	43			
31.2	60.0	42	72.7	0.506	0.995
	75.0	35			
	82.0	32			
	91.0	26			
47.1	61.0	30	58.0	0.469	0.999
	80.0	20			
	90.0	16			
	96.0	13			
55.0	61.0	20	43.6	0.389	0.995
	75.0	16			
	81.0	12			
	91.0	8			
62.5	68.0	11	31.1	0.310	0.968
	76.0	7			
	81.0	5			
	96.0	2			

Prediction Model

The extent of browning at any given time, t, was calculated on the basis of Equations 1 and 9 for the lag ($t \leqslant t_{lag}$) and post-lag ($t > t_{lag}$) periods respectively. With t_{lag} as per Equation 8, and the effect of temperature as per Equation 2, the prediction model reads:

For $0 \leqslant t \leqslant t_{lag}$

$$\int_{B_o}^{B_{LM}} \frac{dB}{B} = \int_{o}^{t} K_L \exp(-E_{aL}/RT)\, dt \qquad (12)$$

with K_L and E_{aL} as per Equations 4 and 3 respectively.

For $t > t_{lag}$

$$B = B_{LM} + (t - t_{lag})\, K_o \exp(-E_a/RT) \qquad (13)$$

with K_o and E_a as per Equations 11 and 10, respectively.

Table 3. Effect of temperature and solids content on the rate, Arrhenius coefficients and Q_{10} of browning formation at the post lag period. (K_o expressed as O.D./min)

Solids Content (°Bx)	Temperature (°C)	$k \times 10^4$ (O.D./min)	Arrhenius Coefficients			Q_{10} 70–80°C
			Ea (Kcal/mole)	ln (K_o)	−r	
11.2	61.0	3.0	15.15	14.731	0.999	1.88
	80.0	11.0				
	95.0	24.5				
31.2	60.0	3.0	15.13	14.894	0.983	1.88
	75.0	9.6				
	82.0	17.3				
	91.0	20.5				
47.1	61.0	4.7	17.15	18.121	0.987	2.04
	80.0	16.5				
	90.0	28.4				
	96.0	63.3				
55.0	61.0	4.4	19.73	22.004	0.999	2.28
	75.0	14.5				
	81.0	23.6				
	91.0	51.0				
62.5	68.0	10.7	23.77	28.234	0.997	2.69
	76.0	21.3				
	81.0	42.5				
	96.0	148.1				

The model was tested in two cases: (a) typical pasteurization and cooling of hot-pack grapefruit concentrate; (b) an industrial concentration process (TASTE evaporator, Gulf Machinery, Florida; for sequence of operations, see Table 4). Figures 5 and 6 show good agreement between predicted and actual values of the extent of browning for both cases.

CONCLUSION

A prediction model was established for the extent of browning in grapefruit juice concentrate during thermal and concentration processes. The model combines the effects of temperature and solids content on the extent of browning in the lag and post-lag periods. The model was tested successfully on two typical commercial processes.

Table 4. Time-temperature concentration data for grapefruit juice in TASTE (10,000 lb/hr) evaporator

Operation Sequence	Time (s)	Concentration (°Bx)	Temperature (°C)
Pre-heating	20	11.0	25 → 80
1st stage	50	15.2	80 → 65
Pasteurization	60	15.2	96
2nd stage	50	24.3	96 → 80
3rd stage	35	40.1	80 → 65
4th stage	50	48.8	65 → 50
5th stage	45	61.0	50 → 45
6th stage + flash cooling	130	62.6	45 → 35 → 8

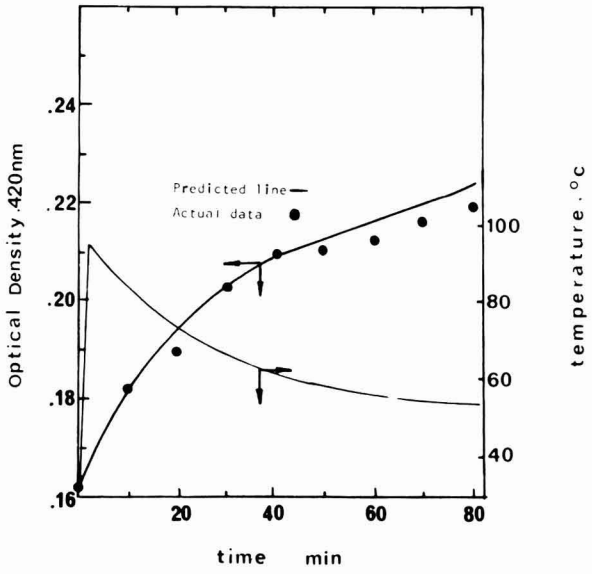

FIG. 5. ACTUAL VERSUS PREDICTED BROWNING IN 52.6°Bx HOT-PACKED GRAPEFRUIT CONCENTRATE

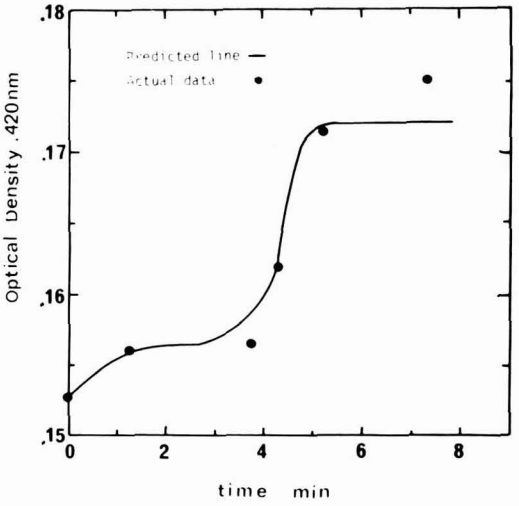

FIG. 6. ACTUAL VERSUS PREDICTED BROWNING IN COMMERCIAL CONCENTRATION OF GRAPEFRUIT JUICE

REFERENCES

BERK, Z. 1976. *Braverman's Introduction to the Biochemistry of Foods*, Elsevier, Amsterdam.

CLEGG, K. M. and MORTON, A. D. 1965. Carbonyl compounds and the non-enzymatic browning of lemon juice. J. Sci. Food Agric. *16*, 191.

ESKIN, X. A. M., HENDERSON, H. M. and TOWNSEND, R. J. 1971. Browning reactions in foods. In *Biochemistry of Foods*, Academic Press, London.

KAREL, M. and NICKERSON, J. T. R. 1964. Effects of relative humidity, air and vacuum on dehydrated orange juice. Food Technol. *18*, 1214.

MEYDAV, S., SAGUY, I. and KOPELMAN, I. J. 1977. Browning determination in citrus products. J. Agr. Food Chem. *25*, 602.

REYNOLDS, T. M. 1965. Chemistry of nonenzymatic browning II. Adv. in Food Res. *14*, 167.

SAGUY, I., KOPELMAN, I. J. and MIZRAHI, S. 1978. Simulation of ascorbic acid stability during heat processing and concentration of grapefruit juice. J. Food Process Engineering 2, 213–225.

WATER SORPTION, REDUCTION OF CAKING AND IMPROVEMENT OF FREE FLOWINGNESS OF POWDERED SOY SAUCE AND MISO

MITSUTOSHI HAMANO and HIROSHI SUGIMOTO

Central Research Laboratories
Kikkoman Shoyu Co., Ltd.
399 Noda, Chiba, Japan

Received for Publication November 16, 1978

ABSTRACT

Water sorption isotherms for powdered soy sauce and miso are similar to those of orange juice and custard powder. Powdered soy sauce showed a powdery condition below 20% RH, caked in the range of 20–33% RH but it easily broke and had an easily free flowing condition. At above 40% RH, powdered soy sauce showed high hygroscopicity and had a non-free flowing condition.

Powdered miso was an easily broken cake in the range of 40–45% RH but at 50% RH, it demonstrated a very hard caked condition. At above 55% RH, powdered miso showed the wet hygroscopic condition and a non-free flowing condition. In addition the reduction of caking of powdered soy sauce by addition of fatty acids was studied and the improvement of free flowingness of both powders with aliphatic hydrocarbons of 5 to 9 carbon atoms was also investigated.

INTRODUCTION

The development of flowing properties in dried powdered foods are important and deserve much more attention, since flow is involved in many processes such as conveyance, pumping and packaging as well as storage. The physical properties of powdered foods may be greatly affected by changes such as caking, hardening, stickiness, shrinkage and hygroscopicity.

Labuza (1968, 1970, 1975) and Duckworth (1976) have discussed the importance of knowledge of the state of water both for processing and stability of dehydrated foods. Rockland (1969) also reported that equilibrium relative humidity or water activity is more closely related to food product stability than total moisture content.

Karel (1975) has discussed the water uptake of amorphous sugar

with a change to crystalline sugar during exposure to increased water activity. Simatos (1975) reported that the hygroscopic character and caking ability of dried products with a high sugar content are ascribed to the amorphous state of sugars. Makower and Dye (1956) reported that amorphous sucrose exhibited slight caking at 24.0 and 28.2% relative humidity (RH) however, caking with some shrinkage at 33.6% RH was predominant. They also showed that glucose held above 4.6% RH caked badly and shrank very markedly. This illustrated how a small change in moisture can affect a food. Notter *et al.* (1959) showed that after 50 h storage at 117°F, air-packed orange juice powder (1.4% moisture) had formed a hard cake, whereas vacuum-packed powder only formed an easily broken cake with a moisture value of 1.3%. Siddappa and Nanjundaswamy (1960) investigated the relationship between cake formation and equilibrium relative humidity of fruit juice and custard powder. For all the products studied except mango custard powder, there was visible cake formation in the range of 2.3–2.8% (45–67% RH, at 37°C) moisture level. The higher moisture level of 4.4% (32% RH) for caking in the case of mango custard powder can be attributed to the presence of additives like starch and skim milk powder.

With respect to this study, powdered soy sauce is added in soup mixes, sauce mixes and gravy mixes for flavor enhancement. Powdered miso is used for making an instant miso soup. Both powdered soy sauce and miso cause trouble in processing and storage since they are non-free flowing, develop caking and are highly hygroscopic (Hamano *et al.* 1972, 1973, 1974, 1976). This paper reports on the effect of relative humidity on caking, free flowingness and hygroscopicity of both powdered soy sauce and miso. In addition the reduction of caking of powdered soy sauce by addition of fatty acids was studied and the improvement of free flowingness of both powders with aliphatic hydrocarbons was also investigated.

MATERIALS AND METHODS

Materials

Short chain aliphatic hydrocarbon (5 to 9 carbon atoms) and saturated fatty acids with 14 to 18 carbon atoms (Tokyo Kasei Kogyo Co., Tokyo), soluble starch (potato), D-glucose and sodium chloride (Wako Pure Chemical Industries, Ltd., Osaka), skim milk powder (Snow Brand Milk Products Co., Ltd., Tokyo) and shoyu oil (Hamano 1973, 85% (w/w) fatty acids) a by-product from a soy sauce fermentation were used as the additives. Fermented soy sauce was made by blending equal

amounts of steamed soybeans and roasted wheat. Following this *Aspergillus* sp. is introduced and the mixture is cultured for three days. The resulting culture, Koji, is mixed with salt water (25% salt) to make a mash called moromi which is then fermented for from 6 to 12 months. After this the raw soy sauce is separated into shoyu oil and soy cake by pressing and pasteurizing.

The miso production process is as follows: For koji preparation, spores of *Aspergillus* sp. are sprayed on steamed rice and then cultured for about two days. The koji is then mixed with salt water (14% salt) and cooked soybeans. The mixture is packed into a vat or tank for fermentation for from 1 to 3 months and is finally sterilized and packaged. The miso products are classified by color from white to red, and by saltiness depending on its salt content. The red type color miso was used.

Sample Preparation

Fermented soy sauce containing 65% (w/w) of water was prepared in powder form by using the Niro Miner Laboratory spray dryer (Niro Atomizer Co., Copenhagen). In addition soy sauce systems were respectively added with 10% (w/v) of sodium chloride, 20% (w/v) D-glucose and 30% (w/v) of soluble starch, dissolved at 80°C, and then spray dried.

The conditions for spray drying of soy sauce with or without additives were as follows: Inlet temperature 130–134°C, outlet temperature 78–81°C, flow rate 8.5 cc/min and centrifugal atomizer 30,000 rpm. For preparation of miso paste, 2.5 volumes of water were added and the mixture was crushed in a colloid mill into liquid form. The drying conditions for liquid miso were as follows: Inlet temperature 132–136°C, outlet temperature 80–86°C, flow rate 6.8 cc/min and centrifugal atomizer 30,000 rpm.

With respect to anticaking additives, these were added after drying. One percent (w/w) of powdery saturated fatty acids and shoyu oil were added to non-additive powdered soy sauce and well mixed in a mortar for 5 min. Fifty milliliters of aliphatic hydrocarbon were added to 10 g of the non-additive powdered soy sauce and miso. After shaking for 20 min the aliphatic hydrocarbon was separated by evaporation and the sample was then dried over phosphorus pentoxide for 10 days followed by a vacuum oven at 5 mm Hg for 24 h. All the dried powders were held at 11–32% RH at 30°C to reach the various constant moisture contents before the flowing experiments were carried out. The particle size of all powders used were those which passed through an 80 mesh and were retained on up to a 200 mesh screen.

Analytical Techniques

The moisture content of the powders were determined by the vacuum oven method (45°C, 3 mm Hg, 48 h) and also determined by the Karl Fisher method (sample weight 300–500 mg, Karl Fisher Moisture Automatic Apparatus, KFA-1 type, Tsutsui Rikagaku Kikai Co., Tokyo). Total nitrogen was determined by the Kjeldahl method (Yokotsuka 1960). Total sugar was determined by the phenol-sulfuric method (Hodge and Hofreiter 1962) and reducing sugar by Bertrand's method (Yokotsuka 1960) to be expressed as glucose, respectively. Crude fat was measured by Soxhlet method with ethyl ether extract as the solvent. The composition analyses of both powders are shown in Table 1.

Table 1. Analyses of general components in powdered soy sauce and miso[1]

Sample	Sodium Chloride	Total Nitrogen	Total Sugar	Reducing Sugar	Crude Fat
Powdered soy sauce	43.7	4.05	9.94	7.32	—
Powdered miso	22.4	3.57	30.48	22.97	7.08

[1] Figures are the contents in g/100 g of dry solids

Water sorption isotherms of the powdered soy sauce, miso and skim milk powder were measured by the weight equilibrium method (Labuza 1975; Rockland 1960; Gál 1975). The equilibrium moisture content was obtained by exposing about 1–2 g lots of powder in test tubes (3.0 cm × 3.0 cm) to atmospheres of different relative humidities at 30°C (±0.2°C) until the corresponding equilibrium moisture content was reached. Prior to placement in the desiccators, they were dried by heating in vacuum oven at 45°C at 5 mm Hg for 24 h. The following salt solutions were used to control RH %: lithium chloride (RH 11.8), calcium chloride (RH 22.3), magnesium chloride (RH 32.3), potassium chloride (RH 43.2), sodium bromide (RH 55.9).

Determination of Caking

The sample powders showing a range of moisture from 1 to 5% of moisture content were used. The caked samples were prepared as follows: Samples of constant bulk density were placed into a weighed test tube (3.0 cm × 3.0 cm). The tube of the sample was well tapped, tightly sealed with a cap and then held in an air oven at 60°C for 1 h.

To test the effect of temperature on caking, this prepared sample was then held in the air oven at temperatures from 40 to 80°C for 1 h. After heating for 1 h, the sealed sample was held at room temperature (20°C). The caked powder was prepared in a cylindrical shape of 13 to 15 mm in thickness and 25 mm in diameter. The hardness value of each caked sample was then determined with the hardness tester (Kiya Seisakujo Co., Tokyo). The absolute maximum pressure was 10 to 20 kg and the hardness was expressed in terms of g/0.785 cm^2 area of the pressing tip. Samples of a hardness value below 2 g/0.785 cm^2 could be easily broken and had a free flowing condition. The bulk density of the original sample in the same tube was also determined by adding a known amount to a graduated test tube.

Determination of Free Flowingness of Powder

The degree of free flowingness of the powders was determined by measuring the angle of repose (θ) and expressed in terms of tan θ. The determination of angle of repose used the revolving cylinder method (Train 1958). The angle of repose for powder was estimated with the Miwa's apparatus (Takeuchi and Miwa 1970, Revolving Cylinder Apparatus, Tsutsui Rikagaku Kikai Co., Tokyo). A 500 ml glass cylinder (9.5 × 8.0 cm) containing 100–130 g of powder was revolved horizontally at 2 revolutions per min for 5 min in a conditioning room (40% RH at 25°C). As the maximum angle that the plate, makes with the horizontal on rotation of the container increases, the angle of repose decreases, and the free flowingness decreases with the caking condition.

RESULTS AND DISCUSSION

The water sorption isotherms for powdered soy sauce, miso and skim milk powder at 30°C are shown in Fig. 1 indicating the typical type II curves. The water sorption isotherms for powdered soy sauce and miso are similar to those of orange juice and mango custard powder (Siddappa and Nanjundasway 1960). However, both powdered soy sauce and miso are not similar to that of skim milk powder.

Powdered soy sauce showed a powdery condition below 20% RH, caked in the range of 20–33% RH but easily broke and had an easily free flowing condition. Above about 40% RH, powdered soy sauce showed high hygroscopicity (surface wetness) and had a non-free flowing condition. Powdered miso contains fatty acids but powdered soy sauce does not. Powdered miso has an easily broken cake in the range

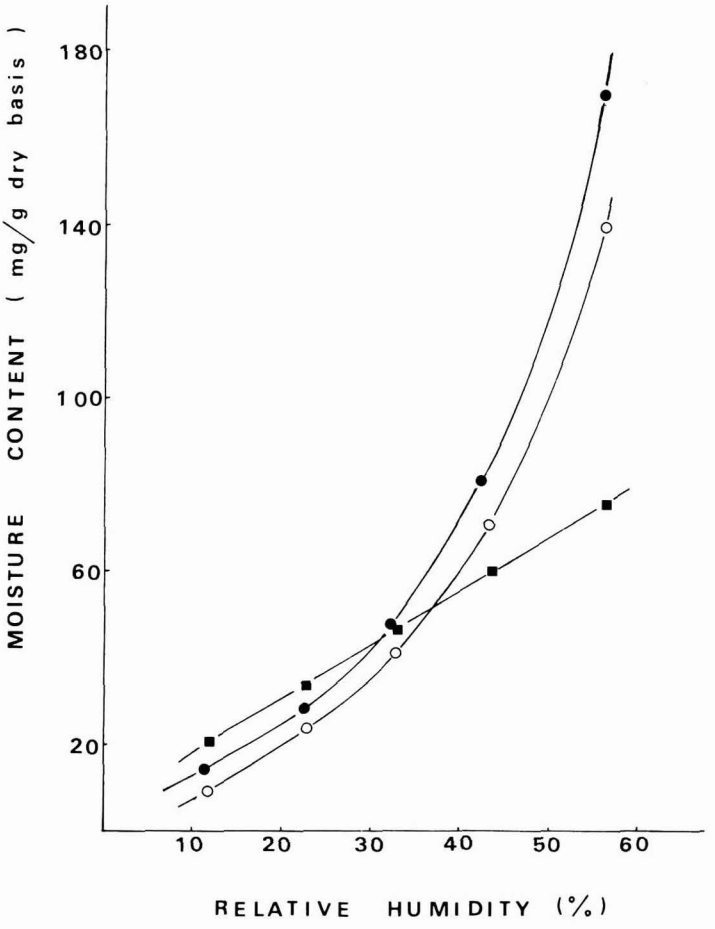

FIG. 1. WATER SORPTION ISOTHERMS AT 30°C
—●— Powdered soy sauce; —○— powdered miso; —■— skim milk powder.

of 40–45% RH but at 50% RH, it demonstrated a very hard caked condition. Above 55% RH, powdered miso showed the wet hygroscopic condition and a non-free flowing condition. The degree of powder caking is affected by the shape of each particle, its size, the moisture content, the bulk density and composition and also by the temperature. The relation between temperature and the degree of caking of the powdered soy sauce is shown in Fig. 2. The degree of caking of the powder increases up to 80°C. The original bulk density of the powder also affects the degree of caking. At above 1.0 g/cc bulk density, the

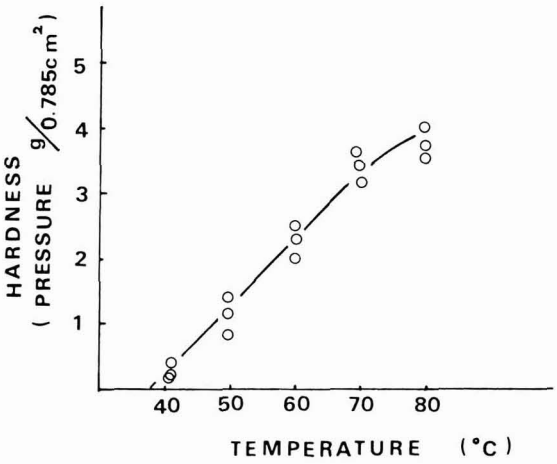

FIG. 2. EFFECT OF TEMPERATURE ON CAKING OF POWDERED SOY SAUCE

The sample with the bulk density 0.875 g/cc and the moisture content 2.3% was used.

degree of caking is very high as shown in Fig. 3. The relation between the particle size and caking of the powder is shown in Fig. 4. The particle size of the sample affected the degree of caking and the highest hardness value was demonstrated within the range of 200–250 mesh particle size.

As for the moisture content in the caked sample, the maximum hardness value was observed within the range of 2.3–3.8% moisture level as seen in Fig. 5. However above 4.7% moisture, the powdered soy sauce became softened or sticky to an extent which made the use of the hardness tester difficult. Figure 5 shows that the degree of caking of powdered soy sauce increased the longer the fermentation period used to prepare the soy sauce was extended.

The maximum hardness value of the caked soy sauce without any additives was observed within the range of 2.3–3.8% moisture level. At the same moisture content, the degree of caking of the powdered soy sauce added with starch was always lower than that of the powdered soy sauce without starch as seen in Fig. 6. The degree of caking of the powdered soy sauce with added glucose showed a greater hardness value than that of the powdered soy sauce with starch. Addition of 1% (w/w) of saturated fatty acids (14 to 18 carbon atoms) and 1% (w/w) of shoyu oil to the powdered soy sauce was very effective in the reduction of the degree of caking as shown in Fig. 7. According to microscopic

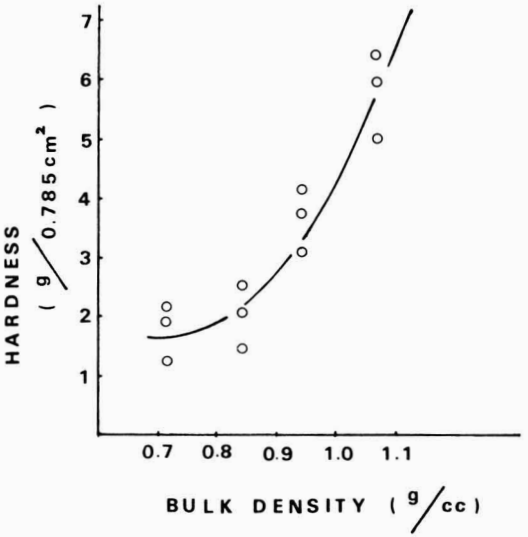

FIG. 3. EFFECT OF BULK DENSITY ON CAKING OF POWDERED SOY SAUCE

The moisture content 2.3% was used.

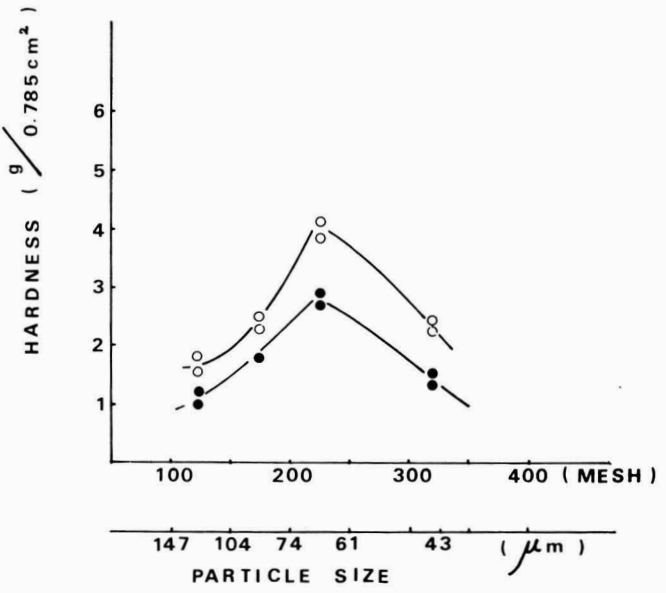

FIG. 4. EFFECT OF PARTICLE SIZE ON CAKING OF POWDERED SOY SAUCE

—○— Moisture content 2.3% — bulk density 0.937 g/cc;
—●— moisture content 2.2% — bulk density 0.937 g/cc.

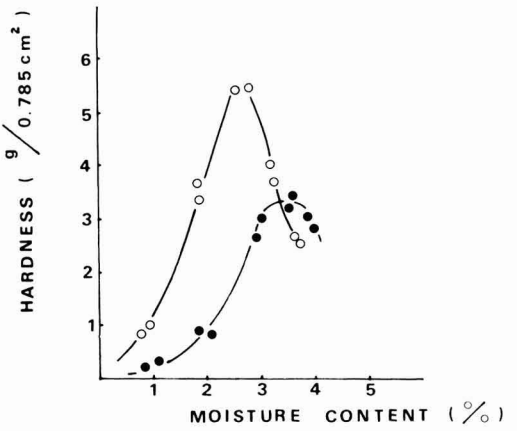

FIG. 5. EFFECT OF MOISTURE CONTENT ON CAKING OF POWDERED SOY SAUCE

—○— Fermented for 6 months — bulk density 0.875 g/cc;
—●— fermented for 1 month — bulk density 0.875 g/cc.

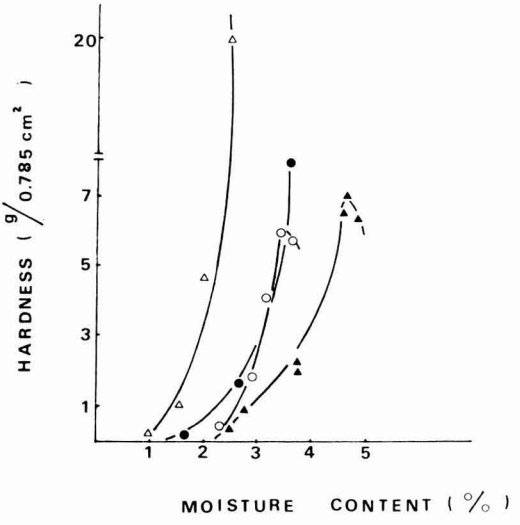

FIG. 6. EFFECT OF GLUCOSE AND STARCH ON CAKING OF POWDERED SOY SAUCE

—○— Non-additive sample — bulk density 0.875 g/cc;
—●— added with sodium chloride — bulk density 0.875 g/cc; —△— added with glucose — bulk density 0.875 g/cc; —▲— added with soluble starch — bulk density 0.875 g/cc.

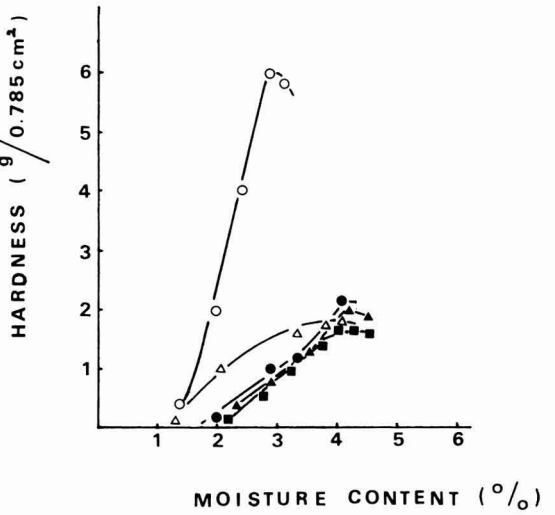

FIG. 7. EFFECT OF FATTY ACIDS ON CAKING OF POWDERED SOY SAUCE

—○— Non-additive sample — bulk density 0.875 g/cc; —△— added with shoyu oil — bulk density 0.875 g/cc; —●— added with myristate — bulk density 0.875 g/cc; —▲— added with palmitate — bulk density 0.875 g/cc; —■— added with stearate — bulk density 0.875 g/cc.

examination, it was suggested that the hydrophobic substances in additives such as fatty acids might attach to the surface of the powder particle and consequently inhibit its caking (Hamano 1973). The powdered miso showed similar behavior. However, the degree of caking was slightly higher than that of powdered soy sauce. According to the water sorption isotherms and Fig. 5 and 6, above 2.0% (20% RH) moisture powdered soy sauce undergoes an amorphous to crystalline transition. Powdered soy sauce and miso usually contain about 6–12% and 14–29% of neutral sugars respectively.

As shown in Table 2 the free flowingness of the powders was considerably improved when aliphatic hydrocarbon of short chains (5 to 9 carbon atoms) were added to the powder. The higher the angle of repose the greater the powder became non-free flowing and entered into the caking condition. At present, the mechanism of improvement of free flowingness by addition of hydrocarbon is not well known. Flink (1975) has indicated that the caking of powders during storage could be due to the partial dissolution of the powder particle which

Table 2. Effect of paraffine oil on flowability of powders

n-Paraffine	Moisture Content (%)	Angle of Repose ($\tan\theta$)[1]
Control[2]	1.87	42.3
+Pentane	1.84	33.0
+Hexane	1.81	29.8
+Heptane	1.78	29.9
+Octane	1.73	30.1
+Nonane	1.82	29.5
Control[3]	2.28	57.1
+Pentane	2.25	51.3
+Hexane	2.43	50.5
+Heptane	2.57	49.8
iso-Paraffine	Moisture Content (%)	Angle of Repose ($\tan\theta$)[1]
Control[4]	1.75	42.7
+Pentane	1.85	33.4
+Hexane	1.88	30.1

[1] Averaged for three repeated tests
[2] Powdered soy sauce
[3] Powdered miso
[4] Powdered soy sauce

resulted in formation of bridges at contact points among the particles. According to his theory, these bridges became solidified during redrying or recrystallization and finally gave structure of increased dimension. Our data possibly supports this if the hydrocarbon prevents contact points.

ACKNOWLEDGMENTS

The authors wish to acknowledge Professor T. P. Labuza for his valuable advice and useful suggestions. The authors also thank Professor S. Koga for his valuable advice and useful suggestions. Appreciation is expressed to Drs. N. Iguchi, F. Yoshida and T. Yokotsuka for their unfailing support and encouragement.

REFERENCES

DUCKWORTH, R. B. 1976. The roles of water in foods. Chemistry and Industry *18*, 1039–1042.

FLINK, J. M. 1975. Application of freeze drying for preparation of dehydrated powders from liquid food extracts. In *Freeze Drying and Advanced Food Technology*, (S. A. Goldblith, L. Rey and W. W. Rothmayr, eds.), pp. 309–329, ,Academic Press, London.

GAL, S. 1975. Recent advances in techniques for the determination of sorption isotherms. In *Water Relations of Foods*, (R. B. Duckworth, ed.), pp. 139–154, Academic Press, London.

HAMANO, M. and AOYAMA, Y. 1973. Effect of saturated fatty acids on hygroscopic equilibria of spray dried soy sauce. J. Agric. Chem. Soc. Jap. *47*, 719–725.

HAMANO, M. and AOYAMA, Y. 1974. Changes of components and behavior of water sorption during spray drying of soy sauce. J. Agric. Chem. Soc. Jap. *48*, 619–625.

HAMANO, M., AOYAMA, Y. and SUGIMOTO, H. 1976. Effect of sugars on water sorption of powdered soy sauce. J. Agric. Chem. Soc. Jap. *50*, 311–317.

HAMANO, M., AOYAMA, Y. and YOKOTSUKA, T. 1972. Moisture sorption of powdered soy sauce. J. Jap. Soc. Food Sci. Technol. *19*, 503–507.

HODGE, J. E. and HOFREITER, B. T. 1962. Determination of reducing sugars and carbohydrates. In *Methods in Carbohydrate Chemistry*, Vol. 1, (R. L. Whistler and M. L. Wolfrom, eds.), pp. 308–394, Academic Press, New York.

KAREL, M. 1975. Physico-chemical modification of the state of water in foods—A speculative survey. In *Water Relations of Foods*, (R. B. Duckworth, ed.), pp. 639–657, Academic Press, London.

LABUZA, T. P. 1968. Sorption phenomena in foods. Food Technol. *22*, 263–272.

LABUZA, T. P. 1975. Interpretation of sorption data in relation to the state of constituent water. In *Water Relations of Foods*, (R. B. Duckworth, ed.), pp. 155–172, Academic Press, London.

LABUZA, T. P., TANNENBAUM, S. R. and KAREL, M. 1970. Water content and stability of low-moisture and intermediate-moisture foods. Food Technol. *24*, 543–550.

MAKOWER, B. and DYE, W. B. 1956. Equilibrium moisture content and crystallization of amorphous sucrose and glucose. Agric. Food Chem. *4*, 72–81.

NOTTER, G. K., TAYLOR, D. H. and DOWNES, N. J. 1959. Orange juice powder. Food Technol. *13*, 113–118.

ROCKLAND, L. B. 1960. Saturated salt solutions for static control of relative humidity between 5° and 40°C. Analy. Chem. *32*, 1375–1376.

ROCKLAND, L. B. 1969. Water activity and storage stability. Food Technol. *23*, 1241–1251.

SIDDAPPA, G. S. and NANJUNDASWAMY, A. M. 1960. Equilibrium relative humidity relationships of fruit juice and custard powders. Food Technol. *14*, 533–537.

SIMATOS, D. and BLOND, G. 1975. The porous texture of freeze dried products. In *Freeze Drying and Advanced Food Technology*, pp. 401–412, Academic Press, London.

TAKEUCHI, K. and MIWA, S. 1970. Measurement of angle of repose and angle of flowing surface in the vacuum various gases. J. Res. Assoc. Powder Technol. Jap. 7, 205–208.

TRAIN, D. 1958. Some aspects of property of angle of repose of powders. J. Pharm. Pharmacol. *10*, 127T–135T.

YOKOTSUKA, T. 1960. Aroma and flavor of Japanese soy sauce. In *Advances in Food Research*, Vol. 20, (C. O. Chichester, E. M. Mrak and G. F. Stewart, eds.), pp. 75–134, Academic Press, New York.

INTENSIVE AGRICULTURAL PRACTICES IN ASIA

JAMES J. RILEY and MERLE R. MENEGAY

The Asian Vegetable Research and Development Center
Shanhua, Tainan 741
Taiwan, Republic of China

Received for Publication November 27, 1978

ABSTRACT

To gain insights into successful cropping systems for possible adoption by other Asian countries, various intensive agricultural practices employed in Taiwan are being studied by the Asian Vegetable Research and Development Center. Primary data are gathered in field trips, farm surveys and interviews with farmers in central and southern Taiwan. Intensive land-use increases the productivity per unit area. Crop diversification enables the farmer to distribute his inputs over several crops and thereby reduce risks. The decentralization of industry in Taiwan provides employment opportunities for farm family members. Food processing factories, located in rural areas, provide the farmer with easily accessible markets for his products. Examples of complementarity of agriculture and industry are given for sweet potato and tomato.

INTRODUCTION

Only one-fourth of Asian rice fields are planted to the new high yielding varieties, first introduced more than a decade ago (International Rice Research Institite 1976). To make the Green Revolution with rice in Asia a success, intensive agricultural practices need to be adopted and multiple crop diversification increased. According to a recent report by the Asian Development Bank, ". . . the Green Revolution on the Japan-Taiwan model is not likely to succeed unless the small farmers of Southeast Asia are prepared to work, as their counterparts in those countries, growing a succession of crops throughout the year," (Asian Development Bank 1971).

For year-round crop production varieties, inputs, and planting dates must be selected which make the best use of the available resources throughout the year. Therefore, tropical research must focus on whole year cropping systems with the aim of intensifying agricultural practices and increasing annual farm productivity.

METHODS

The experiences of Japan and Taiwan with small-scale agriculture are relevant to Southeast Asia and generally provide better guides to the direction the region should go in its agricultural policies and programs, than do the experiences of the United States, Canada, Australia and Western Europe, (Asian Development Bank 1971).

The Asian Vegetable Research and Development Center (AVRDC) is the international agricultural research institute mandated to improve vegetable production in the hot, humid lowland tropics. To achieve its goals AVRDC screens world germ plasm collections of six vegetable crops, namely, tomato, white potato, Chinese cabbage, mungbean, sweet potato, and soybean for desirable traits. Plant breeders combine these into superior plant types suited to a wide range of multiple cropping systems in the tropics (AVRDC 1976).

AVRDC is located in southwestern Taiwan, among some of the most productive and hardest working small farmers in the world. From this vantage point AVRDC scientists, primarily those in the Nutrition, Environment and Management (NEM) Program, gain insights into a wide spectrum of successful cropping systems which may be applicable in other Asian countries (AVRDC 1976). The NEM Program is composed of chemists, agricultural economists, soil scientists, and crop management specialists which give attention to nutritional factors, pesticide residues, post harvest handling, economic production methods, market analysis, cultural techniques, fertilizer utilization efficiency and other topics related to tropical vegetable production.

The data and information contained in this paper were gathered principally by NEM staff members in field trips, farm surveys and interviews with farmers in central and southern Taiwan.

RESULTS

Chinese farmers are renowned for their intensive agricultural methods which they have practiced for centuries (King 1911). Modern farmers in Taiwan have attained their high level of productivity by combining traditional management practices with new technology, including application of chemical fertilizers, pesticides, and herbicides (Department of Agriculture and Forestry (DAF) 1976).

Farms in Taiwan are small by western standards. The average farm in Taiwan is less than one hectare and often is divided into several parcels. Specialized vegetable farms are smaller and have a higher man-land ratio

than other farms in Taiwan. Many growers utilize a distinct cropping pattern on each parcel. Planting techniques include interplanting — one crop planted between the rows of another crop; adjacent planting — single crops planted near one another; relay cropping — one crop planted into a standing crop of another species within a few weeks of harvest; and sequential cropping — succession of crops planted over one or more years which maintain soil fertility and gives the farmer a high aggregate income.

Vegetable crops (e.g. onions, cabbage, tomato) are frequently used in cropping systems with rice and field crops (e.g. soybean, sorghum, corn). The cropping patterns used by two Taiwanese farmers, illustrate the complexity and intensity of the cropping system, Menegay *et al.* 1978.

Farmer Chen's 0.42 ha farm is divided into 2 parcels of 0.18 ha and 0.24 ha (Menegay 1976) which was cropped as follows:

Parcel Size	Cropping Pattern			
	1973			1974
(ha)	June			May
0.18	Late rice /	Snow pea /	Early rice /	Summer melon
0.24	Chinese leek			

Farmer Huang had a 1.5 ha farm divided into 3 parcels of 0.2, 1.0, and 0.3 ha (Menegay 1976) which was cropped as shown below:

Parcel Size	Cropping Pattern			
	1973			1974
(ha)	June			May
0.2	Late rice /	Sweet potato /	Fallow	
1.0	Late rice /	Fallow /	Early rice /	Fallow
0.3	Vegetables			

To analyze the intensive agricultural patterns found in Taiwan, a Crop Intensity Index (CII) was developed by AVRDC which takes into account the area planted and crop length. An index value of 1.0 or

greater indicates high land use efficiency. Farmer Chen's CII equals 1.04 while that for Farmer Huang is 0.72. The CII is described fully in Menegay (1976) and Menegay *et al.* (1978).

In Taiwan, the Ministry of Economic Affairs is responsible for both agricultural and industrial development. This Ministry has Departments of Mining, Commerce, Agriculture and Forestry, Water Conservation, Public Enterprises, and General Affairs as well as a Board of Foreign Trade and an Industrial Development Bureau (China Yearbook 1976). As a result, competition between agriculture and industry is minimized. Industrial plants, including those for processing agricultural products are often located in rural areas.

Sweet potato production and utilization in Taiwan offers one example of the complementarity between agriculture and industry. Taiwan sweet potato production ranks second only to rice as a stable crop in tons produced annually (DAF 1976). Production and utilization patterns in a region are related to the degree of commercialization present.

In commercialized districts, sweet potato production exceeds farm needs for hog feed, since hogs are raised increasingly by moderately large agri-businesses which prefer formulated feed to sweet potato. Most of the farm excess is sold to starch factories, clustered near sweet potato fields (Table 1). The resulting starch has a multitude of uses, including textile sizing, paper coating, paste, and laundry starch[1]. Sale of waste products from the extraction process accounts for 13.5% of the processed output value of the starch factory (Calkins *et al.* 1977). The refuse is collected to produce, via a fermentation process, calcium sulfate and citric acid (Fig. 1). The former is used in the manufacture of cement and the latter for soft drinks.

Another example of synergism between agriculture and industry is illustrated by the tomato processing industry. Processed tomato is the fastest rising agricultural export in Taiwan (Table 2). This industry is based on raw material produced by small farmers. A single factory may process tomatoes harvested from more than 400 farms. Some firms appoint farmer representatives to arrange contracts between the processing factory and individual farmers. The contract guarantees the price the factory will pay for tomatoes produced. These representatives grow and distribute tomato seedlings to farmers (seeds are provided by the processor). Growers receive fertilizer and insecticides from the company via the farmer representative. Charts showing seasonal fluctuation

[1] The local starch industry is declining due to increasing availability of low cost imported starch. In the paper industry it is being replaced by Carboxyl Methyl Cellulose (CMC).

Table 1. Sweet potato production and utilization in Taiwan[1]

	Less Commercialized Districts[2]		Commercialized Districts[3]	
	(kg)	(%)	(kg)	(%)
Production Per Farm	4430	100.0	9069	100.0
On Farm Use[4]	4276	96.5	4240	46.8
Sold	154	3.5	4829	53.2
To: Starch factory	0	0	2946	32.5
Feed mill	0	0	0	0
Local shipper	87	2.0	919	10.1
Hog producer	23	0.5	561	6.2
Neighbors	44	1.0	403	4.4

[1] Source: Calkins *et al.* 1977
[2] Average of data from Changhua and Pingtung districts
[3] Average of data from Tainan and Taitung districts
[4] Almost exclusively for feeding animals

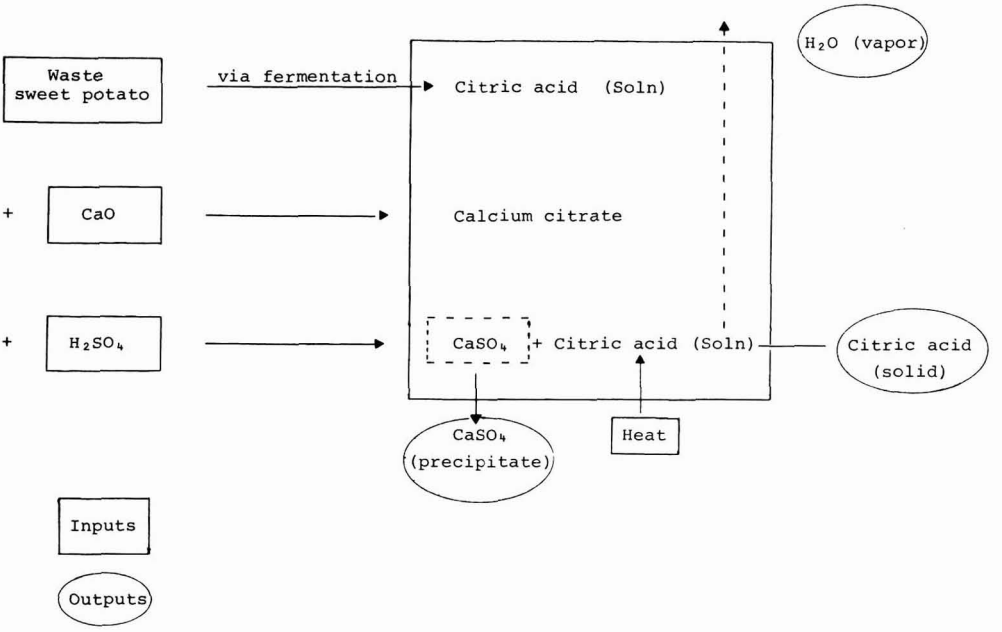

FIG. 1. SCHEMATIC DIAGRAM OF CHEMICAL REACTIONS INVOLVED IN PROCESSING OF SWEET POTATO WASTE PRODUCTS FROM STARCH FACTORY

Table 2. Value of Taiwan processed tomato exports[1]

Year	Export Value (Million of U.S. Dollars)[2]
1970	0.1
1971	0.3
1972	0.4
1973	2.9
1974	9.2
1975	12.3
1976	13.1
1977	15.6

[1] Source: T. C. A. 1970–1978
[2] Figures rounded off to nearest 100,000 U.S. dollars

of major pests and diseases, the recommended chemicals to control them, and other suggested cultural practices are distributed to contract farmers. Other technical assistance is also provided as needed.

Wooden crates for transporting tomatoes to the factory are brought to farmers' fields at harvest time by the farmer representative. Where adequate roads exist, trucks pick up crated tomatoes and deliver them to the factory. Farmers also transport tomatoes to the factory via a variety of motorized and animal drawn vehicles. A standard rate of reimbursement is paid farmers who transport their own produce. In 1977 the exported tomato products were sold mostly within Asia, with over 60% being purchased by Japan (Taiwan Canners Association 1978). Processing waste products are returned to farms to feed hogs, AVRDC (1976).

DISCUSSION

Taiwan is an excellent field workshop in which to observe intensive agricultural practices potentially adaptable to other Asian countries. Intensive land-use increases the productivity per unit area. Crop diversification enables the farmer to distribute his inputs such as fertilizer, labor, and equipment over several crops. This reduces the severity of any one crop failure and promotes a more evenly distributed cash flow throughout the year. Irrigation is required for year-round cropping and the infrastructure must be well developed for the farmer to consistently command a good price for his products.

Decentralization of industry provides employment opportunities for

farm family members and also serves to stem the tide of migration to urban centers. The sociological benefit attached to keeping the oriental family (usually spanning several generations) together cannot be overemphasized.

Food processing factories located in rural areas provide easily accessible markets to the farmer. In order for industry to be located away from ports and the primary points of consumption there must be an efficient, and relatively inexpensive, transportation system for farm goods.

By being located in Taiwan, the Asian Vegetable Research and Development Center is able to observe successful small farm crop production and develop appropriate cultural practices to accompany the superior varieties being bred for the tropics. These packages of technology are evaluated at outreach stations and by national program researchers in other Asian countries. This means of assisting the small Asian farmer shows promise. Only time will tell whether it will prove successful.

REFERENCES

Asian Development Bank. 1971. *Southeast Asia's Economy in the 1970s*, p. 684, Praeger Publishers, New York.

Asian Vegetable Research and Development Center. 1976. Progress Report for 1975, Shanhua, Taiwan, ROC.

Asian Vegetable Research and Development Center. 1976. Tomato Report for 1975, Shanhua, Taiwan, ROC.

CALKINS, P. H., HUANG, S. Y. and HONG, J. F. 1977. Farmers' viewpoint of sweet potato production in Taiwan, Technical Bulletin No. 4, AVRDC, Shanhua, Taiwan, ROC.

China Yearbook. 1976. China Publishing Co., Taipei, Taiwan, ROC.

Department of Agriculture and Forestry. 1976. Agriculture in Taiwan, Taipei, Taiwan, ROC.

International Rice Research Institute. 1976. Research Highlights for 1975, Los Banos, Philippines.

KING, F. H. 1911. Farmers of forty centuries (or permanent agriculture in China, Korea and Japan), p. 441, Reprinted recently from original plates by Rodale Press, Emmaus, Pennsylvania.

MENEGAY, M. R. 1976. Farm management research on cropping systems. Technical Bulletin No. 2, AVRDC, Shanhua, Taiwan, ROC.

MENEGAY, M. R., HUBBELL, J. N. and WILLIAM, R. D. 1978. Crop intensity index: A research method measuring land use in multiple cropping. HortScience *13*(1).

Taiwan Canners Association. 1970, 71, 72, 73, 74, 75, 76, 77 and 78. Taiwan Export of Canned Food, (published annually in August), Taipei, Taiwan, ROC.

MICROSTRUCTURE OF FREEZE DRIED EMULSIONS: EFFECT OF EMULSION COMPOSITION[1]

FREDERIK GEJL-HANSEN and JAMES M. FLINK[2]

Department of Nutrition and Food Science
Massachusetts Institute of Technology
Cambridge, Massachusetts 02139

Received for Publication December 13, 1978

ABSTRACT

The physical relationship between lipid and dried solid matrix was studied by microscopic methods. Oil-in-water emulsions were prepared with the lipid concentration and structure-forming solute in the aqueous phase being varied. Methods to quantitatively evaluate the distribution of the lipid phase with respect to the dry matrix material (i.e. encapsulated versus surface lipid) are presented. The degree of encapsulation of the fat phase in the matrix was shown to depend on morphological characteristics of the solid matrix components and lipid concentration. The microscopic methods reported here also give a picture of the interrelationship of the oil and solid matrix in freeze dried oil-in-water emulsions so that the physical location of fat can be related to product and process parameters. This information will be important for interpreting results of product performance and stability studies of dried fat-containing food products, and to aid in designing improved dehydrated emulsion-based engineered foods.

INTRODUCTION

The utility of freeze dried multicomponent products, such as emulsified systems, depends on the product being stable during storage and rehydratable to a state which is essentially equal to the original emulsion. The extent to which the quality of the emulsified system is retained in the final product will depend on changes in the interactions between the various components of the multiphase system during the freeze drying process.

---

[1] Contribution Number 3065 of the Department of Nutrition and Food Science, Massachusetts Institute of Technology, Cambridge, Massachusetts

[2] Present address: Department for the Technology of Plant Food Products, The Royal Veterinary and Agricultural College, DK-1871 Copenhagen V, Denmark

Schmidt Walters (1968), Lladser *et al.* (1968) and Lladser and Arancibia (1972) indicate that the physical location of the oil and its interaction with the solid support could be important factors in explaining various properties of freeze dried oil-in-water emulsions. Two extreme cases describing oil locations in a dried emulsion are (1) fully encapsulated as oil globules or (2) thin surface deposits on the solid support (Gejl-Hansen and Flink 1976; Buma 1971).

The ratio between free oil and encapsulated oil will determine various physical properties of the dried product such as reconstitutability, stickiness and free flowability of the powdered product, and creaming and foaming behavior of the rehydrated product. This results since the position of the oil in a given support will determine the hydrophobic-hydrophilic character of the product and therefore, its wettability and dispersibility (Buma 1971; Beyerlein 1972a,b).

To describe the structure of freeze dried oil-in-water emulsions and in particular the location of the oil relative to the support material, it has been necessary to utilize multiple microscopic techniques, as well as to develop some suitable chemical extraction methods (Gejl-Hansen and Flink 1976). The development of these techniques allows evaluation of the ratio of encapsulated to free fat and the effect that process variables such as oil concentration and solid support material and concentration have on this distribution.

For example, oil concentration relative to solids concentration may influence the ratio between encapsulated fat and free fat. Lladser *et al.* (1968) showed that with higher oil concentration (above 10% oil for 13.3% solids), their emulsion broke during freeze drying. It has been shown that following freeze drying of emulsions containing crystallizing or crystalline solutes, the oil globules are located as a film on the surface of the crystalline solids (Gejl-Hansen and Flink 1976) whereas it has been shown with lipids (Buma 1971; Gejl-Hansen and Flink 1976) and flavor components of low solubility (Flink and Gejl-Hansen 1972; Flink *et al.* 1973; Massaldi and King 1974) that insoluble droplets can be incorporated into an amorphous matrix during drying processes. It can be expected that a higher concentration of amorphous forming solute would give more matrix into which oil globules can be incorporated and thus presumably a higher fraction of the lipid encapsulated.

In the study reported here, the distribution of oil between encapsulated and surface locations has been evaluated for a variety of freeze dried powders prepared from different solutes. For some of these support materials, the effect of oil phase volume on lipid distribution was also determined.

MATERIALS AND METHODS

Preparation of Samples

Oil-in-water emulsions were prepared with either triolein or linoleic acid. Solid supports which were present in the aqueous phase are listed below:

Support	Type	Source
Maltodextrin (DE = 15)	Soluble carbohydrate	Grain Processing Co.
Maltose	Soluble disaccharide	Fisher Chemical Co.
Carboxy methyl cellulose (CMC)	Soluble cellulose gum	Hercules Chemical Co.
"Soluble" starch	Polysaccharide	Merck
Avicel	Microcrystalline cellulose	FMC Corp.
Gelatin	Protein	Difco Labs
Egg albumin	Protein	Mann Research Labs
Glycine	Crystallizing amino acid	Fisher
Urea	—	Calbiochem

Emulsifiers (Span 80 and Tween 80 at a 1:2 ratio) were used at a concentration of 9% of the oil phase. The emulsion systems were prepared by first blending the oil and Span 80 together, and then adding this mixture to an aqueous solution or dispersion of the solute material and Tween 80. The emulsification was carried out by high speed mixing in a Sorvall Omnimixer for 10 min before adding the oil phase.

After emulsification the emulsions were transferred to trays, frozen at −20°C, then hard frozen at liquid nitrogen temperature (−196°C), and freeze dried as slabs of about 5 mm thickness.

Extraction of Lipid Phase

Sequential extraction methods for quantitative evaluations of surface and encapsulated lipid were used. In the first step, a soxhlet extraction using hexane is carried out for 8 h to remove surface fat from the freeze dried emulsions. (Microscopic observation of powder structure before and after this hexane extraction was used to ensure that no changes in powder structure occurred. Potential structural transformations were avoided by operating the soxhlet at a low reflux rate.) Residual hexane in the dry powder was removed by evacuation for about 1 h. Surface oil

extracted by the hexane was determined gravimetrically following vacuum evaporation of the hexane solvent and final drying at 50°C in a vacuum oven.

The extracted powder is then dispersed in water in a separatory funnel to disrupt the carbohydrate matrix and release the encapsulated oil. Chloroform was added and the funnel was shaken. Ethanol was added to improve the sharpness of the interface between the water and the chloroform phases. The amount of the ethanol required depends on the concentration of oil, solids, water and chloroform. If desired, phase separation can be accelerated by holding the separatory funnel at 4°C for a few hours. The aqueous phase is re-extracted two times and the chloroform phases pooled. The oil present in the chloroform-ethanol solvent is also determined gravimetrically after vacuum evaporation of the solvent phase followed by drying overnight in a vacuum oven at 50°C The total fat content of a freeze dried sample is also obtained using the water-chloroform-ethanol extraction. Total oil content determinations were in excellent agreement with the sum of the oil contents determined for the surface and encapsulated lipid fractions.

Microscopic Methods

The various microscopic methods used have been described in detail by Gejl-Hansen and Flink (1976).

Optical Microscopy (OM). Transmitted bright field microscopy was conducted on ground and flaked samples, immersed in either a drop of immersion oil (α-bromonaphthalene or paraffin oil) or, when the rehydrated condition was desired, in water as the immersion medium. Surface deposits of fat in the freeze dried emulsions were visualized by staining the unsaturated bonds of freely available lipids (i.e. surface) with osmic acid vapors (Buchheim *et al.* 1974; Gejl-Hansen and Flink 1976). The degree of darkening (light brown to black) depends on the surface oil concentration, degree of lipid unsaturation, and exposure time (usually 10–40 min). Microscopic observations showed that in cases where there was encapsulated oil it is protected by the impermeable matrix and does not react with the osmic acid vapors.

Scanning Electron Microscopy (SEM). Small flakes of dried emulsion were attached to the aluminum SEM specimen holders with double sided adhesive tape or silver paint. The samples were then coated with a thin layer of aluminum or gold (approximately 100–400 Å) in a Bendix vacuum evaporator (Model CVC-14). A JEOL JSM-U3 scanning electron microscope was operated at 15–25 Kv. Secondary electrons were detected and used for image formation.

Electron Microprobe (EMP). The electron microprobe was used to

detect surface oil in the osmium stained freeze dried oil-in-water emulsions. Following osmic acid treatment and OM observation, a coating with aluminum, and subsequent SEM observations, the coated samples are transferred to the electron microprobe and observed at an accelerating voltage of 15 Kv and a beam diameter of about 3–5 μ. Image formation is based on the intensity of the M_α X-ray line of osmium (λ = 6.49 Å) so osmium-rich areas (i.e. surface fat) appear as concentrations of bright dots on a dark background. Aluminum was used for coating since one of the M X-ray lines of gold interferes with the osmium signal. If desired, the sample can be transferred back to the SEM or OM for further morphological studies.

RESULTS AND DISCUSSION

Effect of Matrix Forming Solids on Freeze Dried Emulsion Structure

Triolein emulsions were prepared using a variety of matrix forming solutes. The freeze dried materials were subjected to microscopic evaluations using OM, SEM, and EMP in combination with osmic acid staining. Table 1 summarizes the principal results.

Avicel

Since Avicel is insoluble in water the homogenized dispersion contains oil globules together with rods and shredded pieces of cellulose crystals. Thus, emulsions containing microcrystalline cellulose (Avicel) as the solid support show a different type of emulsion structure than that observed with most other solutes examined. A typical sample contains oil globules in a size range of less than 1 μ to 8 μ and cellulose crystals anywhere from a few microns on the edge to 100 μ. After freeze drying, microscopic examination shows the emulsion structure to be a dense network of cellulose crystals, but with no oil visible. In the SEM the characteristic wrinkled surfaces of the larger crystals is easily noted. This network structure of cellulose crystals is only obtained when the aqueous dispersion has been mixed at high speed in the Omnimixer prior to addition of the oil phase. The shredding of the larger cellulose crystals produces smaller filaments, which have a bridging effect between the larger crystals resulting in a dense matrix structure. If this shredding step is omitted the freeze dried sample appears as the original free flowing powder. In the OM (Fig. 1) the freeze dried emulsion shows the Avicel crystals, but again no oil is visible. Since

Table 1. Microscopic evaluation of freeze-dried triolein emulsions

	Total % Oil on Dry Basis	Matrix Structure	Incorporated Oil Droplets	Droplets Upon Rehydration	Sticky Surface	OsO_4 Stain	EMP Image
Avicel	23	Microcrystals	None	Yes, large	Yes	Very dark	None
CMC	70	Flexible plates not smooth (SEM)	Many small	Some	No	Light	Weak
Egg albumin	20	Flaky platelets	numerous tiny	Yes	No	Dark	Weak
Gelatin	33	Hard honeycombed network	Many tiny	Matrix swells slow release	No	White	None
Glycine	20	Anisotropic plates needles	No	Yes, many large	Very	Very black	None
Maltodextrin	20	Plates	Many	Yes, many	Yes	Dark	Strong
Maltose	20	Plates	Many	Yes, many	Yes	Dark	Strong
Starch	20	Intact granules	None	Many large appear	Very	Very dark	None
Urea	20	Needles	Small only	Many, also large	Yes	Very dark	None

FIG. 1. SCANNING ELECTRON MICROSCOPE VIEW OF 4.5% LINOLEIC ACID, 15% AVICEL FREEZE DRIED EMULSION (COATED WITH GOLD) (400X)

Table 2. Effect of triolein phase volume on encapsulation following freeze drying

Emulsion Composition[a]		Oil Encapsulated	
g Oil / g Maltodextrin	% (w/w) of Oil in Fresh Emulsion	g Oil / g Maltodextrin	% of Total Oil
0.026	0.51	0.002	8
0.053	1.05	0.004	8
0.130	2.60	0.013	10
0.250	5.00	0.021	8
0.510	10.21	0.056	11

[a]All fresh emulsions contained 20% (w/w) maltodextrin

amorphous cellulose material is not observed in either the OM or SEM, no oil could be encapsulated. Soxhlet extractions recovered all the oil (i.e. as free fat) (Table 2).

All the oil present was also isolated when the water-chloroform-

ethanol extraction was used. Since neither method changes or disrupts the cellulose structure, all oil must be present as surface fat. Upon exposure to osmic acid vapors a strong reaction indicative of surface oil was obtained. Practically all surfaces are covered by oil due to the high fat concentration. It should be mentioned that pure Avicel does not react with osmic acid. Good EMP observations are not possible with Avicel systems because the curved surfaces of the microcrystals cause the osmium X-ray signals from the fat deposits to be scattered and not caught by the detector, thereby preventing image formation.

Carboxymethyl Cellulose (CMC)

Fresh emulsions of CMC were made at a concentration of 0.5% w/w so that the viscosity of the aqueous solution would be similar to the other systems tested. Even with 1.15% w/w oil, the freeze dried emulsion showed only slight reaction with osmic acid, indicating that most of the oil phase is incorporated in the CMC matrix. This oil fraction is visible as a dense distribution of small oil globules in flexible plates of the solid CMC. In the EMP only scattered and weak signals were observed.

Figure 2 shows an SEM of the CMC emulsion. It was noted that areas of the platelet surface are quite rough, with small holes penetrating the surface. Using sequential OM, SEM and EMP techniques as described by Gejl-Hansen and Flink (1976), it was demonstrated that these holes gave pathways for contact of the "encapsulated" droplets with the environment. This contact probably accounts for the light OsO_4 staining and weak EMP signals.

Egg Albumin

Fresh emulsion of egg albumin contained numerous oil droplets having an average size of less than 1 μ. The freeze dried structure consists of platelets with an abundance of tiny oil inclusions (Fig. 3). These droplets are released upon addition of water to the dried matrix, and the oil size distribution is still less than 1 μ. This might be attributed to the emulsifying properties of the egg albumin itself. Exposure of the egg albumin emulsion to osmic acid gives spots of dark staining and additionally a uniform weak stain over the whole surface. However, the product is termed "non-sticky." The EMP for the egg albumin samples shows no locally stained areas, but rather a uniform weak signal intensity over the whole surface. This indicates that the staining reaction which took place was due not only to possible minor surface fat from the added oil but also to residual fat naturally present in the commer-

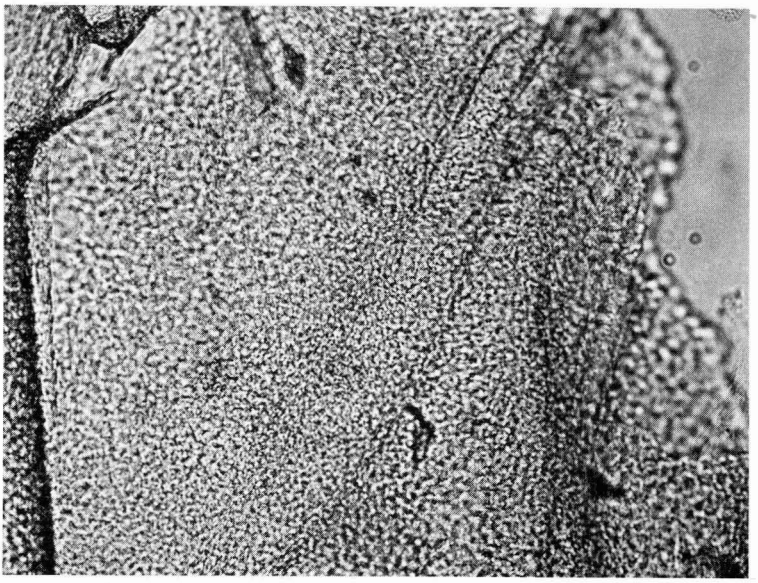

FIG. 2. OPTICAL MICROSCOPE VIEW OF 1.15% LINOLEIC ACID, 0.5% CMC FREEZE DRIED EMULSION (400X)

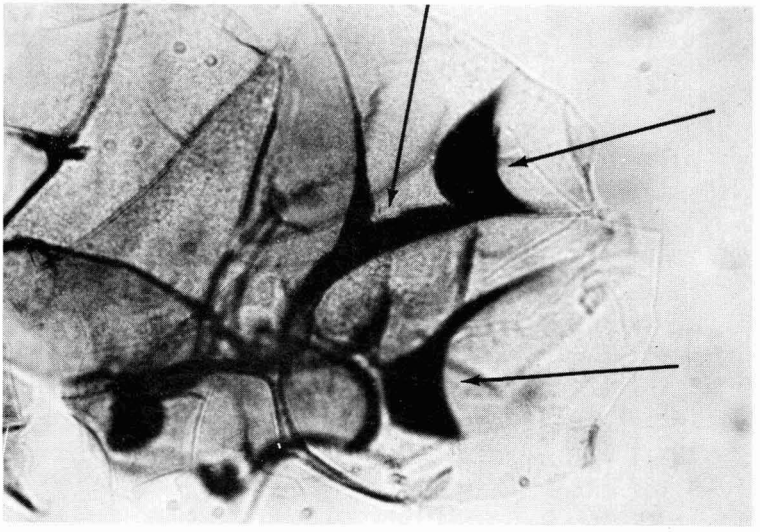

FIG. 3. OPTICAL MICROSCOPE VIEW OF 5% LINOLEIC ACID, 20% EGG ALBUMIN FREEZE DRIED EMULSION, EXPOSED TO OsO_4 VAPORS (400X)

cial egg albumin. A test showed that pure egg albumin will react somewhat with osmic acid.

Gelatin

The freeze dried matrix of triolein and gelatin showed a very characteristic network structure. The smooth platelets that build up this network were observed to contain numerous tiny oil inclusions (Fig. 4), which are only released very slowly in water as the matrix swells. The freeze dried emulsion is non-sticky and has no reaction with osmic acid, and no signal in the EMP. By microscopic analyses, it can be seen that gelatin was able to incorporate the oil, nearly quantitatively.

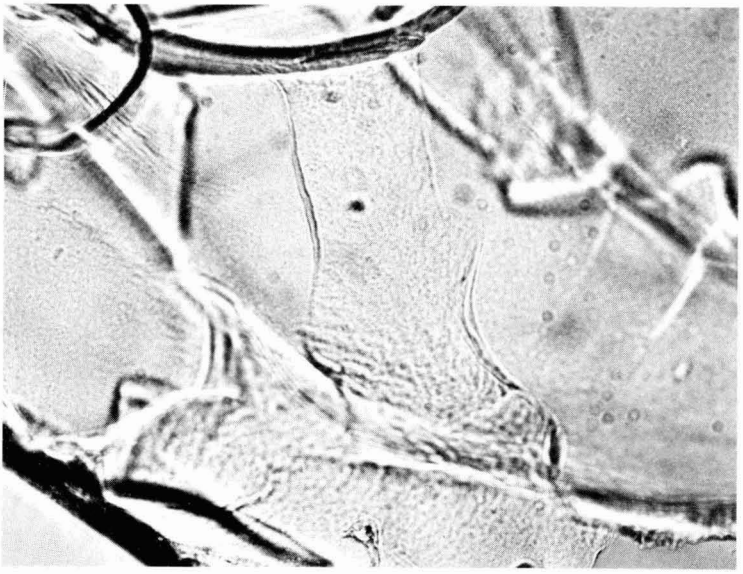

FIG. 4. OPTICAL MICROSCOPE VIEW OF 1.25% LINOLEIC ACID, 2.5% GELATIN FREEZE DRIED EMULSION (400X)

Glycine

When fresh glycine-based emulsions, which contained well dispersed one micron oil droplets, were freeze dried, no oil is observed to be incorporated in the glycine phase. This is due to the fact that glycine does not form a concentrated amorphous phase during freezing, but rather a crystalline phase which totally excludes the oil droplets (Fig. 5). In the freeze dried state surface oil is never observed as

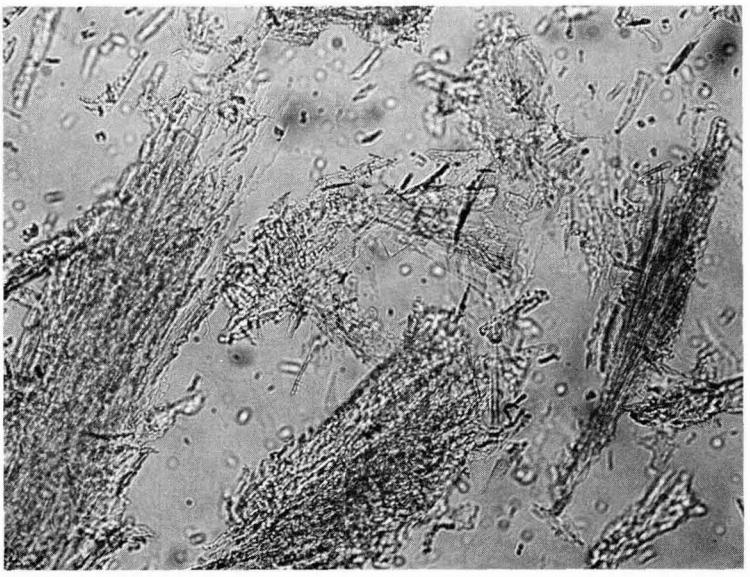

FIG. 5. OPTICAL MICROSCOPE VIEW OF 5% LINOLEIC ACID, 20% GLYCINE FREEZE DRIED EMULSION (400X)

droplets since surface energy affects favor spreading of the oil. Exposure of the freeze dried glycine emulsion with its extensive surface oil to osmic acid gives a very dark staining reaction. The dried emulsion also has significant "stickiness." These facts indicate that the oil is present as a surface coating on the glycine crystals. Upon rehydration, the released oil globules are many times larger than the original one-micron average diameter. The SEM shows the matrix to consist of thin needles and plates. No EMP image is observed since many needles are smaller than the probe diameter (1–3 μ) and the needle geometry sends emitted X-ray signals away from the detector.

Maltodextrin

The freshly prepared emulsions had maximum oil droplet diameters of about 1 to 2 μ. The dried emulsion was noted to be very porous. In the optical microscope nearly all maltodextrin grains were smooth, with thicknesses averaging 8–12 μ. The grains contained spherical oil inclusions of diameters $\leqslant 10\ \mu$ (Fig. 6). The relatively high content of surface oil was easily demonstrated by exposing dried grains to osmic acid vapors (Fig. 7 and 8). It can be noted that concentrated staining occurred along surface characteristics (i.e. surface depressions due to ice

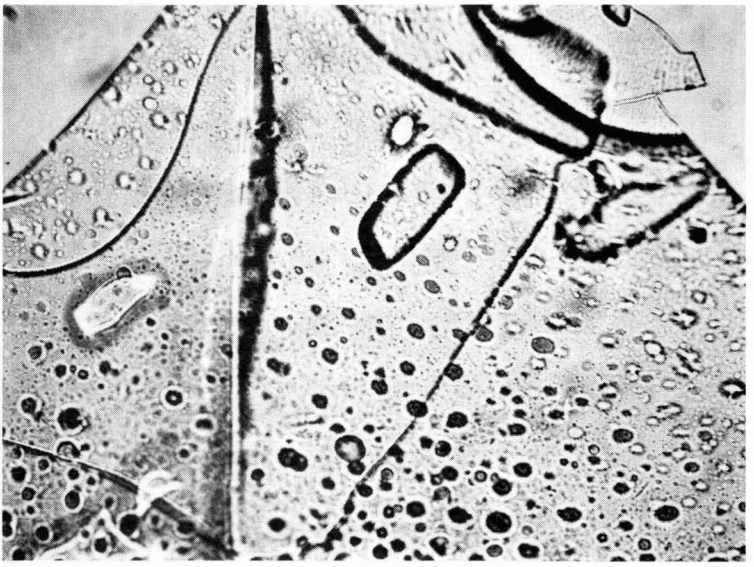

FIG. 6. OPTICAL MICROSCOPE VIEW OF 5% TRIOLEIN, 20% MALTODEXTRIN FREEZE DRIED EMULSION (400X)

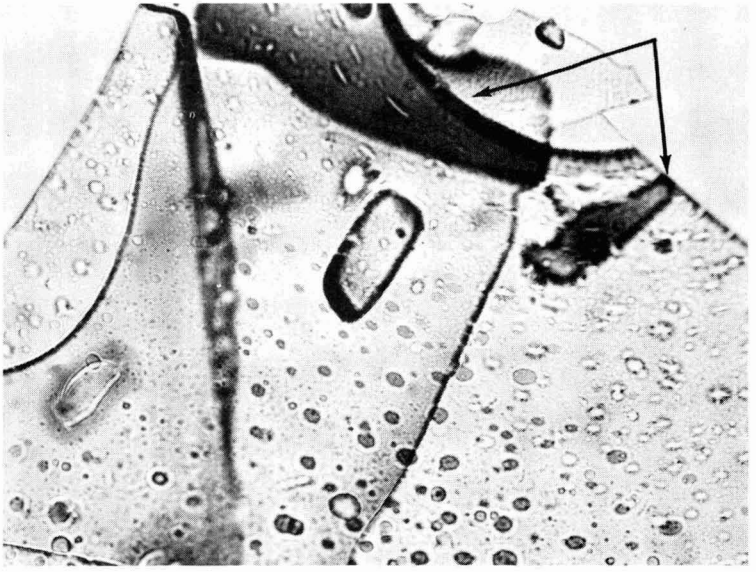

FIG. 7. OPTICAL MICROSCOPE VIEW OF SAME FIELD AS FIG. 6 AFTER EXPOSURE TO OsO_4 VAPORS. NOTE STAINING ALONG SURFACE DEPRESSIONS DUE TO ICE DENDRITES (600X)

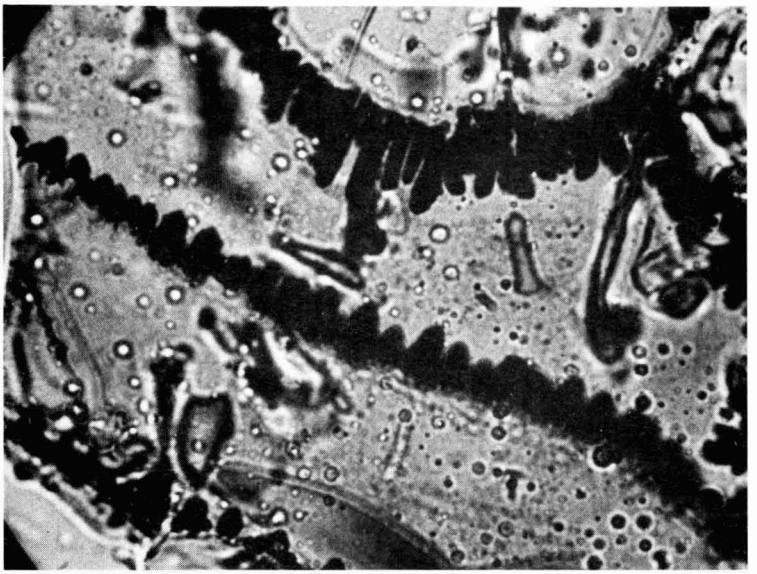

FIG. 8. OPTICAL MICROSCOPE VIEW OF 1% LINOLEIC ACID, 20% MALTODEXTRIN FREEZE DRIED EMULSION, EXPOSED TO OsO_4 VAPORS. NOTE STAINING ALONG SURFACE DEPRESSIONS DUE TO ICE DENTRITES (600X)

dendrites, grooves, ridges between platelets, etc.).

While rehydration gave a dispersion having globule diameters around 1–2 μ, a number of droplets having larger diameters (up to 35 μ) were observed. Rehydration of freeze dried emulsion which had its surface oil removed by the soxhlet extraction gave average globule sizes still around 1–2 μ, but no droplets were larger than 12 μ, the thickness of the maltodextrin plates.

Maltose

Maltose-based emulsions showed different structural appearances which depended on the ability to conduct the freeze drying process without "collapse." "Collapse" is the viscous flow of the matrix which results from combinations of sample temperatures and moisture contents being above critical values (Bellows and King 1972, 1973; MacKenzie 1966; Tsourouflis *et al.* 1976). In the liquid state prior to freezing, the emulsion had an essentially uniform oil droplet size of about 1 μ, though a few larger droplets of up to 10 μ diameter were noted. The droplets were well dispersed, with no tendency to cluster.

When samples underwent partial collapse during freeze drying, this could be observed macroscopically by the appearance of glossy areas,

yellow areas (oil), and in some instances foam crusts. Under the optical microscope, oil inclusions, air inclusions, and holes were observed. Oil globules which were present in the fresh emulsion, but which were larger than the average grain thickness (9 μ) were not observed in the dry matrix. The appearance of many holes in the freeze dried maltose grains is an indication of the viscous flow (collapse) which occurred during freeze drying.

A typical grain structure for a maltose emulsion which freeze dried with collapse is shown in Fig. 9 (exposed to osmic acid). To be noted are the discontinuous staining areas, such as around the edge of hole (A), staining of "eggshell" area (B), and weaker staining at large depressions (C), which still include oil droplets in the bottom wall.

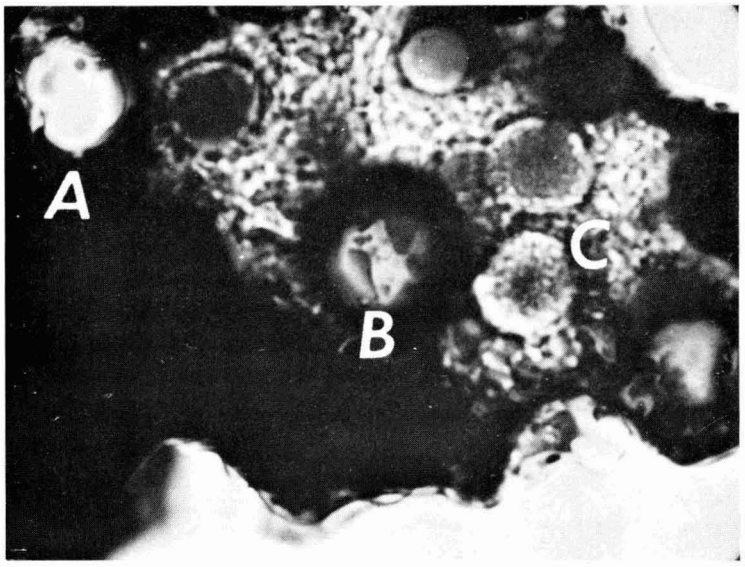

FIG. 9. OPTICAL MICROSCOPE VIEW OF 3.75% LINOLEIC ACID, 15% MALTOSE FREEZE DRIED EMULSION (COLLAPSED), EXPOSED TO OsO_4 VAPORS (600X)

A. hole; B. "eggshell"; C. depression with thin bottom.

In the SEM the rounded form of the partially collapsed freeze dried emulsion, with its wrinkles, holes, and depressions, is noted (Fig. 10). In the OM view of the grain (Fig. 11) it is possible to see the rounded edges, the holes, and the unbroken large depressions ("eggshells") which appear lighter since they are much thinner (1–3 μ) than the rest

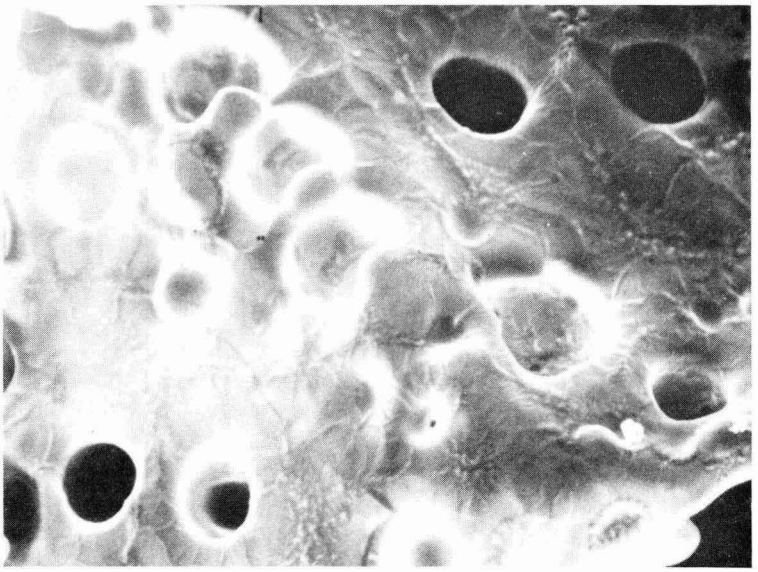

FIG. 10. SCANNING ELECTRON MICROSCOPE VIEW OF 3.75% LINOLEIC ACID, 15% MALTOSE FREEZE DRIED EMULSION (COLLAPSED) (COATED WITH ALUMINUM) (320X)

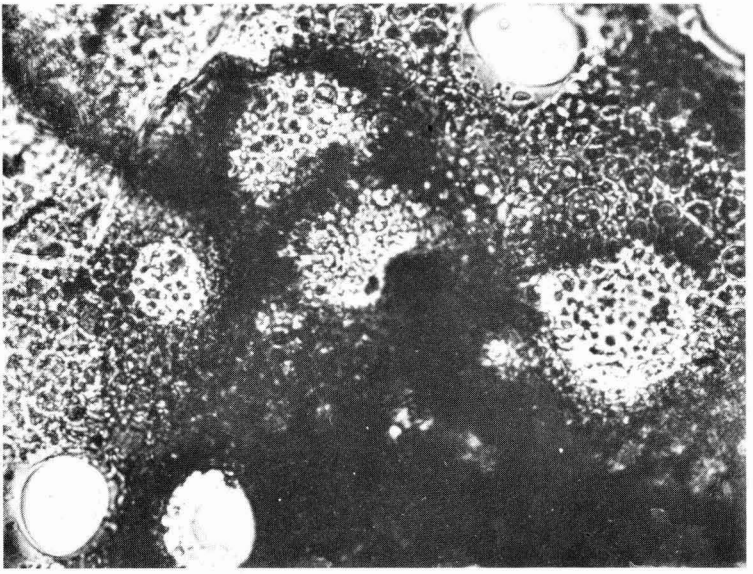

FIG. 11. OPTICAL MICROSCOPE VIEW OF SAME FIELD AS IN FIG. 9 (400X)

of the grain, which is about 8–10 μ thick. It can be seen that the walls of the "eggshells" contain oil inclusions. When freeze drying was conducted so that the freeze dried cake showed no macroscopic areas of melting or collapse, the OM (Fig. 12) showed a dense concentration of encapsulated globules. It is also noted that the grain structure was significantly different in appearance from that of the maltose emulsions which had undergone collapse; the edges of the grains were not rounded, but rather straight, and holes, depressions, and "eggshells" were very few in number. Exposure to osmic acid vapors showed surface fat as distinct, but discontinuous deposits, generally of much smaller size than the large pools of surface fat encountered for the collapsed emulsion sample. The rehydrated emulsion shows most oil globules to be larger than present in the original, which was less than 1 to 2 μ. Many oil globules have diameters ranging from 10 to 30 μ.

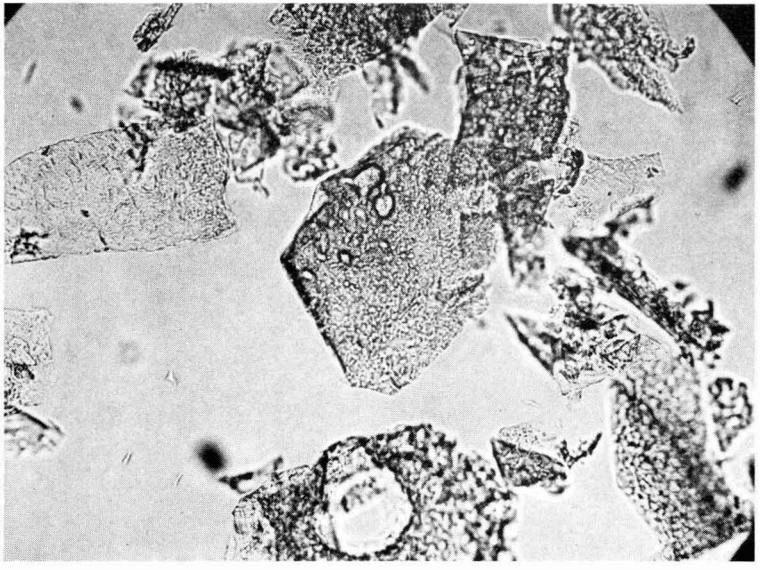

FIG. 12. OPTICAL MICROSCOPE VIEW OF 3.75% LINOLEIC ACID, 15% MALTOSE FREEZE DRIED EMULSION (NON-COLLAPSED) (150X)

Starch

Emulsions of "soluble" starch were freeze dried and observed for lipid location. Upon microscopic examination, the matrix was found to consist of clusters of intact starch granules with no visible amorphous

phase, indicating that the starch had not been heated sufficiently to be gelatinized during preparation. No oil was incorporated in the starch granules; no droplets were visible. However, the very sticky matrix reacted strongly with osmic acid and SEM (Fig. 13) showed oil bridges between granules at locations which would give especially dark staining. It was also noted that large lenses of oil would appear upon addition of water. This indicates that the fat is present as a surface layer on the granule. No EMP image could be obtained since the spherical fat-coated granules do not give good directional reflection of the X-rays towards the detector.

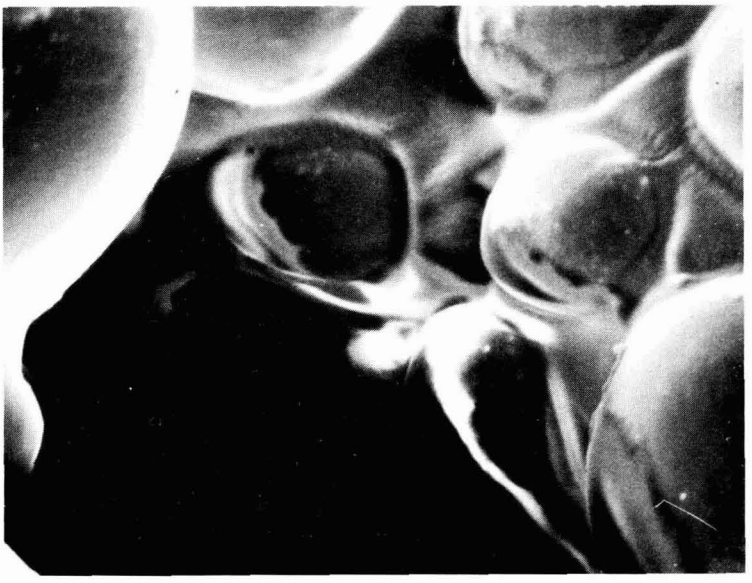

FIG. 13. SCANNING ELECTRON MICROSCOPE VIEW OF 5% LINOLEIC ACID, 20% STARCH FREEZE DRIED EMULSION, EXPOSED TO OsO_4 (COATED WITH ALUMINUM) (1500X)

Urea

The specific interaction of urea with certain lipid materials when prepared from solution is well known (Martinez Moreno and Vasquez Roncero 1964). There is one report that in a urea-based freeze dried emulsion the lipid phase was present as discrete droplets external to the crystalline urea needles (Lladser *et al.* 1968). Urea samples were therefore prepared by precipitation from saturated methanol solutions and by freeze drying of aqueous emulsified systems.

Samples were prepared by adding the following lipid materials to a methanol solution saturated with urea: (a) no lipid present, (b) triolein and (c) linoleic acid. The oil concentration was about 3% of the urea-methanol solution which had been decanted from the saturated solution so that no undissolved urea was present. No precipitation of urea was noted in the lipid-free samples, unless some of the methanol was evaporated. Triolein is not solubilized by the methanol and thus was present on the bottom of the flask as distinct oil globules around which there was a slow precipitation of urea during a 24-h period. In the linoleic acid sample, precipitation was rapid, occurring within a minute.

Microscopic investigation of the urea crystals recovered from the methanol solutions showed a distinct difference in the crystal morphology. The pure urea formed short rods while the oil-containing urea samples appeared as long slender needles with visible oil inclusions. These observations show that linoleic acid, and, to a lesser extent triolein, form urea adducts which have a needle-like morphology.

Urea freeze dries to give a crystalline solid in the form of clusters of short rods or needles. The morphological pattern of the urea crystals is contrained by the limited growth space in the eutectic caused by the already formed ice crystals. Therefore comparisons of the crystal morphology of these freeze dried samples with the above mentioned oil-urea-methanol systems should be done very cautiously.

When aqueous solutions of urea (20% w/w) containing triolein (1%, 3%, 5% w/w) were freeze dried, small oil droplets (diameters $\leqslant 1\ \mu$) were observed to be trapped within the crystalline structure. These oil droplets were not dissolved when the freeze dried urea samples were subjected to the hexane extraction. Addition of water gave solution of the urea crystals, resulting in the appearance of large numbers of oil droplets having a wider range of diameters (up to $10\ \mu$) than has been observed in the dried systems. When exposed to osmic acid vapors, the freeze dried triolein-urea systems turn dark, with samples having higher oil phase volumes giving stronger reaction. Samples washed in hexane (which did not change the matrix structure) did not react with the osmic acid. These facts, together with the observed stickiness of the dry particles suggests that oil is also present on the surface.

Freeze dried samples of urea (20%) and linoleic acid (1%, 5%) show very much the same morphological patterns as mentioned above for triolein-urea emulsions. The urea forms needle-like structures with lipid inclusions generally 1 to $2\ \mu$ in diameter (Fig. 14). It appeared that the linoleic acid systems contained fewer visible droplets than the corresponding triolein systems which is not surprising considering its potential for adduct formation. Upon exposure to osmic acid vapors the 1%

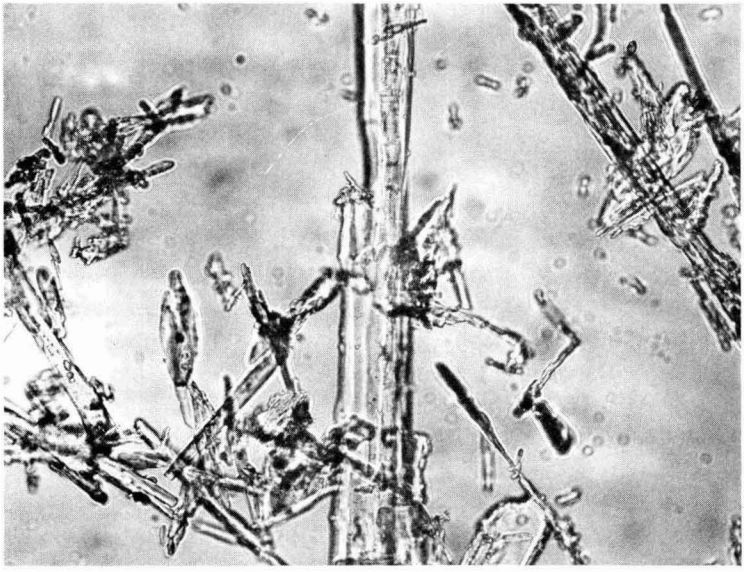

FIG. 14. OPTICAL MICROSCOPE VIEW OF 5% LINOLEIC ACID, 20% UREA FREEZE DRIED EMULSION (400X)

linoleic acid sample show no staining, indicating that all the oil was present in the adduct. The 5% linoleic acid sample showed little or no staining upon prolonged exposure to osmic acid indicating that the urea (20%) was still able to encapsulate practically all the oil, leaving essentially none as free surface fat.

When freeze dried urea-linoleic acid samples, or hexane-washed urea-triolein samples (i.e. surface oil removed) were rehydrated, oil globules with diameters much larger than observed in the dried sample were noted. Droplet diameters up to 12 μ were not unusual. In this case the mechanism of dissolution of the urea crystals results in the occluded lipid being released under conditions which foster potential coalescence, thus giving the observed increase in maximum droplet size.

Influence of Oil-Solid Ratio on Degree of Encapsulation in Freeze Dried Emulsions

Maltodextrin emulsions (20% w/w solids) containing triolein at 0.5 to 10% w/w levels were quantitatively evaluated for oil distribution by Soxhlet hexane extraction (surface fat) and water-chloroform-ethanol extraction (encapsulated fat). Optical microscopy showed that density of inclusions in the matrix was increasing with increasing oil

concentration, though the samples appeared similar for oil concentrations above 1%. Similar observations were found for linoleic acid based emulsions. The amount of fat encapsulated in the maltodextrin was found to increase with oil concentration (Table 2). Table 2 also shows that for the range of triolein:maltodextrin ratios examined, the encapsulated oil was about 10% of the total oil present in the system. This is significant since it indicates that while 100% encapsulation was never observed, even at low oil concentrations (0.05 g oil per g maltodextrin) emulsion samples could be prepared with an amount of oil encapsulated which was greater than the total amount of oil present in the low oil concentration systems. For example, while the emulsion containing 0.51 g oil per g maltodextrin has an amount encapsulated (0.056 g oil per g maltodextrin) which is higher than the total amount of oil present in the 0.026 g oil per g maltodextrin emulsion, only 8% of the latter emulsion's oil was encapsulated.

Quantitative Measures of Lipid Distribution

Table 3 gives quantitative measures of the distribution of lipid (triolein or linoleic acid) for systems of maltodextrin, Avicel or maltose. For 3 of the maltodextrin samples the influence of initial lipid phase volume on the amount encapsulated is similar to that noted in Table 2. These 3 samples have a high surface oil concentration, in agreement with the information presented in Table 1 for maltodextrin emulsions.

On one occasion, however, a maltodextrin-linoleic acid emulsion at a high lipid phase volume (5.5% w/w) gave a high degree of encapsulation as measured by the hexane Soxhlet extraction. The high degree of encapsulation was confirmed by optical microscopy. Very dense concentrations of deformed oil globules were observed in practically all maltodextrin grains (Fig. 15). It should be noted that these oil inclusions are present as individual droplets, and not as undefined discontinuities. The majority of the grains appeared flat and smooth (also confirmed by SEM). Exposure of dried grains to osmic acid gave only scattered darkening, with the staining generally associated with areas having a rough surface topology, such as ridges, depressions, grooves and closely spaced parallel flakes. The EMP showed signs of low intensity only along these topological features, confirming low surface fat concentrations.

This high degree of encapsulation could not be repeated in several subsequent attempts, and it is not known what particular factors resulted in the high encapsulation this one time. Evaluations using maltodextrins of other DE values, on the chance that a formulation error was

Table 3. Lipid distribution in freeze dried emulsions

Emulsion[a] Composition	g Oil / 100 g Dry Emulsion	Surface[b] Oil	Encapsulated[b] Oil	g Oil Encapsulated / g Carbohydrate
1.1% linoleic acid 20% maltodextrin	5.2	79	21	0.012
5.5% linoleic acid 20% maltodextrin	21.6	26	74	0.204
2.0% triolein 20% maltodextrin	9.1	80	20	0.020
5.1% triolein 20% maltodextrin	20.3	90	10	0.026
0.75% linoleic acid 15% Avicel	4.8	100	0	0
4.5% linoleic acid 15% Avicel	23.1	100	0	0
3.75% linoleic acid 15% maltose	20.0	88	12	0.030
3.75% linoleic acid[c] 15% maltose	20.0	97	3	0.008

[a]Concentrations in (w/w)
[b]Percentage of total oil
[c]Collapsed during freeze drying

made failed to yield a high level of encapsulation. It can be speculated on the basis of observations made that some change in the emulsifier system resulted in an emulsified system which was more stable to freezing drying stresses than the usual system. While not a conclusive indication that the emulsifier is responsible, it is interesting that the "droplets" can be stabilized as individual units with such extensive geometric deformation. It is also interesting that contrary to behavior noted earlier for samples showing distorted droplets (Gejl-Hansen and Flink 1976) the surfaces of platelets of this emulsion show no holes due to penetration of droplets.

The Avicel systems show that 100% of the oil is present as a surface layer, which agrees with all the powder characteristics noted above.

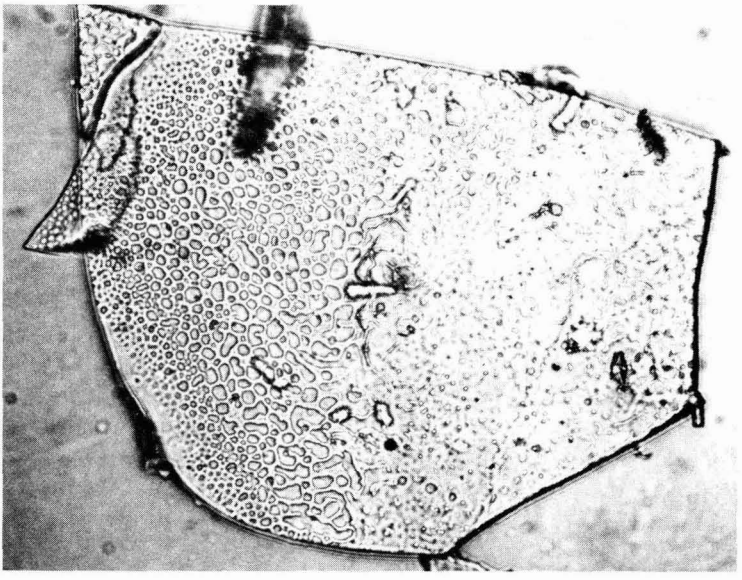

FIG. 15. OPTICAL MICROSCOPE VIEW OF 5.5% LINOLEIC ACID, 20% MALTODEXTRIN FREEZE DRIED EMULSION (400X)

As noted above, freeze dried maltose samples were obtained with or without collapse occurring. These samples were found to have different extents of oil encapsulated, with collapse resulting in an increase of surface oil (Table 3). This results since collapse is the phenomena of viscous flow of the matrix. In the process of drying, if the matrix conditions are such that the matrix is somewhat plastic, then vapor formed in the matrix can deform the maltose matrix elements giving rise to expanding films. If the vapor expands sufficiently so that it breaks through both sides of the maltose phase, holes will be formed, while if one film yields first, a large depression with a thin bottom results (Fig. 11). When this flow of the maltose matrix occurs, the encapsulated droplets are subjected to shear stresses which deform them from their spherical shape, which together with the formation of new surface and matrix elements of decreased thickness results in localized breakthrough and spreading of the formerly encapsulated oil phase. The fact that collapse has occurred does not mean that spillage of encapsulated oil must occur. Thus, while heavy OsO_4 staining occurs at the edges of holes and the thin films in the bottoms of the large depressions are lightly stained, there are some encapsulated droplets remaining in the thin films, and much of the matrix shows numerous encapsulated droplets (Fig. 9).

CONCLUSION

The above results show how the fate of the oil phase is dependent on whether it can be incorporated in an amorphous solute (egg albumin, gelatin, CMC) during freezing or excluded when the matrix forming solute is an insoluble crystalline solid (starch) or crystallizes as water is removed from the solution (glycine). The results show that a macroscopic observation termed "stickiness" correlates qualitatively very well with osmic acid staining as seen in the OM. Furthermore, the darkness of the osmic acid staining was found to correlate very well with EMP image strength except in the case of adverse matrix structure geometries (glycine and starch).

It was noted that levels of encapsulation never reached 100%, even if at low phase volumes of oil, such that the total amount of oil present was much less than the amount which could be encapsulated by the matrix-forming solute, if it had been freeze dried from an emulsion with a higher phase volume of oil.

ACKNOWLEDGMENTS

The authors acknowledge the support of this work by HEW/PHS (Grant No. FD 00713-02). One of the authors (FGH) thanks Westreco, Inc. for financial support. The authors also wish to acknowledge the contribution of Mr. William Phipps.

REFERENCES

BELLOWS, R. J. and KING, C. J. 1972. Freeze drying of aqueous solutions: Maximum allowable operating temperatures. Cryobiology *9*, 550–561.

BELLOWS, R. J. and KING, C. J. 1973. Product collapse during freeze drying of liquid foods. AIChE Symposium Series No. 132. *69*, 33–41.

BUCHHEIM, W., SAMHAMMER, E. and LEMBKE, J. 1974. Die Lichtmikroskopisch Sichtbarmachung von Fett auf der Oberflasche von Milchpulverteinchen. Milchwissenschaft *29*(9), 513–517.

BUMA, T. J. 1971. Free fat and physical structure of spray dried whole milk. Ph.D. Thesis, Agricultural University of Wageningen.

FLINK, J. and GEJL-HANSEN, F. 1972. Retention of organic volatiles in freeze-dried carbohydrate solutions: Microscopic observations. J. Agr. Food Chem. *20*, 691–694.

FLINK, J. M., GEJL-HANSEN, F. and KAREL, M. 1973. Microscopic investigations of the freeze drying of volatile-containing model food solutions. J. Food Sci. *38*, 1174–1178.

GEJL-HANSEN, F. and FLINK, J. M. 1976. Application of microscopic techniques to the description of structure of dehydrated food systems. J. Food Sci. *41*, 483–489.

LLADSER, M. and ARANCIBIA, A. 1972. Microphotographic study of lyophilization of oil-in-water emulsions. J. Pharm. Pharmac. *24*, 404–406.

LLADSER, M., MEDRANO, C. and ARANCIBIA, A. 1968. The use of supports in the lyophilization of oil-in-water emulsions. J. Pharm. Pharmac. *20*, 450–455.

MACKENZIE, A. P. 1966. Basic principles of freeze drying for pharmaceuticals. Bull. Parenteral Drug Assn. *20*, 101–129.

MARTINEZ MORENO, J. M. and VAZQUEZ RONCERO A. 1964. The application of urea inclusion compounds in fat analysis. In *Analysis and Characterization of Oils, Fats and Fat Products*, (H. A. Boekenoogen, ed.), pp. 95–118, Interscience, London.

MASSALDI, H. and KING, C. J. 1974. Volatiles retention during freeze drying of synthetic emulsions. J. Food Sci. *39*, 438–444.

SCHMIDT WALTERS, J. 1968. Lyophilization of oil-water emulsions. Ann. Fac. Quim. Farm., Univ. Chile.

TSOUROUFLIS, S., FLINK, J. M. and KAREL, M. 1976. Loss of structure in freeze-dried carbohydrate solutions: Effect of temperature, moisture content and composition. J. Sci. Food Agric. *27*, 509–519.

TRANSPORT OF OXYGEN THROUGH ICE AND FROZEN MINCED FISH

JAMES M. FLINK[1] and MARK GOODHART

Department of Nutrition and Food Science
Massachusetts Institute of Technology
Cambridge, Massachusetts 02139

Received for Publication December 13, 1978

ABSTRACT

The storage life of frozen fish depends, in part, on quality degradation due to oxidation of lipids. In minced fish products, transport of oxygen through the frozen material is one possible mechanism for supplying the required oxygen to the reactive lipids. Oxygen transport through ice and minced fish at −5°C was determined using a Clark-type oxygen electrode in a sample of known geometry. Oxygen permeability of ice appeared related to physical defects of the ice samples. Fast frozen ice had widely varying permeability values, while slow frozen ice varied over a more narrow range. Ice thickness and annealing procedures affected observed permeability values. Slow frozen minced fish was more permeable to oxygen than slow frozen ice, and coating of the minced fish with a slow frozen ice glaze resulted in reduced oxygen transport.

INTRODUCTION

The mincing process is used to prepare fish flesh suitable for modification into salable products, such as fish cakes or fish sticks, from fish species which normally have little or low market value. The marketability of these minced fish blocks and the fish products produced from them is dependent on their storage life. An important factor in determining the storage life of frozen fish products is the deterioration in quality associated with lipid oxidation.

Fish lipids are especially reactive because of the presence of highly unsaturated fatty acids (Olcott 1962). The lipid oxidation reaction requires oxygen and for extensive rancidity to develop, it is necessary

[1] Present address: Department for the Technology of Plant Food Products, The Royal Veterinary and Agricultural College, DK-1871 Copenhagen V, Denmark

Journal of Food Processing and Preservation 2 (1978) 229–248.

that a substantial source of oxygen be available in contact with the tissue lipids. This can result from oxygen being present *in situ* at the reaction sites, or by the transport of oxygen from the environment to the reaction sites. In the case of minced fish, there is also the possibility of incorporation of oxygen into the product during the mincing process and/or in packaging. This is especially important since the oxygen comes into contact with a large surface area of fish undergoing tissue breakdown and presumably release of heme-type compounds, which have a known catalytic effect on lipid oxidation (Tappel 1962; Olcott 1962). Thus, the minced fish can be considered a well mixed combination of lipid, oxygen and catalyst. Removal of heme-bearing tissues is an area of much study at present (Dingle and Hines 1975; Miyauchi *et al.* 1976).

Among the methods presently used for retarding oxidative rancidity are surface applications of ice glazes (Tarr 1947; Tarr 1948; Bauernfeind 1953; Andersson and Danielson 1961) or protective calcium alginate gels (Glicksman 1969). These methods are premised on the glazes serving as a barrier to oxygen diffusion and the assumption of the absence of *in situ* oxygen. Studies reporting on the effectiveness of ice or gel glazes have not involved quantitative evaluation of oxygen transport, but rather were generally based on evaluation of oxidative behavior, or organoleptic scores after various times of storage. In order to develop optimized strategies for surface treatments to retard oxidative rancidity and extend storage life, it is necessary to develop information regarding the transport behavior of oxygen through the basic material (minced fish) and the proposed coating materials. In addition, the relationship of oxidation potential due to oxygen transport versus *in situ* oxygen (both natural and incorporated) must be known.

While ice may be thought of as being a relatively impermeable material, El-Sherbieny (1969) indicated that air "entrapped" in frozen material can pass out through micropores when placed in a low pressure environment. Jellinek (1967) reviewed information available on the presence of liquid-like layers on ice surfaces. The possibility that these liquid-like layers could serve as media to transport materials was investigated by Riehl *et al.* (1973). They showed that the ice blocks were crossed by a number of physical defects, such as cracks, or air inclusions, in which a luminescent dye, uranin, was transported. In studies on the physical adsorption of vapors on ice, transport into ice specimens had been proposed as one explanation to account for uptake of the vapors beyond monolayer coverage. Postulated pathways include fine cracks, or clathrate formation and their transport (Adamson *et al.* 1967; Adamson and Jones 1971). Lambert *et al.* (1973a,b) have shown

that n-butanol can be transported through fast-frozen ice. Again their results have been interpreted in terms of physical defects in the ice structure. Numerous studies have been reported on the state of water in frozen tissue, especially from the point of view of the so-called "unfreezable water" (Duckworth 1971; Charm and Moody 1966; Karel 1975). Recently, Storey (1970) and Kent (1975) have reported on the diffusion behavior of water in frozen tissue in terms of diffusion through the unfrozen water layer.

A Clark-type oxygen probe system has been used to evaluate the oxygen permeability of ice (fast frozen and slow frozen) and a calcium alginate gel, materials often used in industrial processes to exclude oxygen from packaged fish. The oxygen permeability of frozen minced fish flesh has also been measured, along with the changes in permeability due to application of an ice glaze, or which might occur in storage due to surface dessication associated with "freezer burn."

MATERIALS AND METHODS

Oxygen Probe Design

Electrodes measuring oxygen partial pressure as a function of current output were constructed according to the design of Johnson *et al.* (1964). They consisted of a silver-lead system placed behind a teflon membrane (Fig. 1). The electrolyte was 0.5N sodium acetate in a 5N acetic acid solution.

Glass tubing (6 mm in diameter) formed the body of the probe. Silver wire (20/1000 in. diameter) which was wound into a tight spiral large enough to cover the end of the glass tubing, formed the positive terminal. Lead foil (1/32 in. thick), cut into strips 1/16 in. × 5 in. formed the anode. Solder joints were insulated by pieces of 1/32 in. diameter PVC tubing which had been swollen in chloroform. When the chloroform evaporated, the PVC tubing shrunk to form a tight fit around the exposed joint.

A teflon membrane (1 mil thick) was stretched over the silver cathode and held tightly in place by a piece of tight fitting PVC tubing. The tip of the lead anode is placed approximately 1/8 in. from the silver cathode. The probe is filled completely with the acetic acid-sodium acetate electrolyte and the top end sealed off with epoxy.

Probe current was read on a digital microammeter. Average probe output at room temperature was approximately 15×10^{-6} amps.

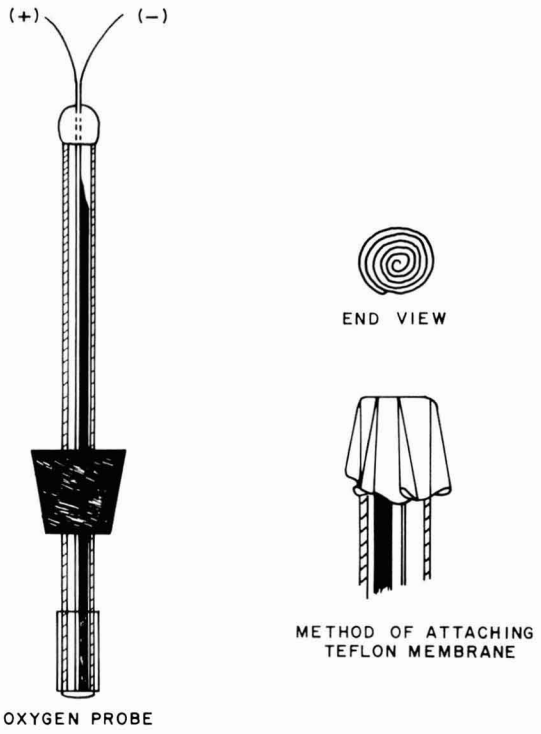

FIG. 1. SCHEMATIC DIAGRAM OF OXYGEN PROBE

Sample Preparation

To prepare fast frozen ice, the probe was first dipped into liquid nitrogen to chill it, and then the cold probe was rapidly dipped into ice water for a very short period of time so as to form a layer of ice. The probe was re-cooled in the liquid nitrogen and then re-dipped in the ice water. This process was repeated until the desired ice thickness was achieved. During the freezing process, sharp noises indicative of the ice cracking were noted. The ice was also observed to be cloudy. The fast frozen samples were then placed into a controlled temperature chamber.

For the remaining types of samples, an integral oxygen probe-sample assembly used a rubber stopper on the probe body to hold the 1 in. diameter cylindrical copper sample holders (Fig. 2). Sample material was placed inside the copper jacket with the probe tip near the open end of the copper jacket. Thickness of the sample was adjusted by moving the probe up or down in the stopper-copper jacket assembly.

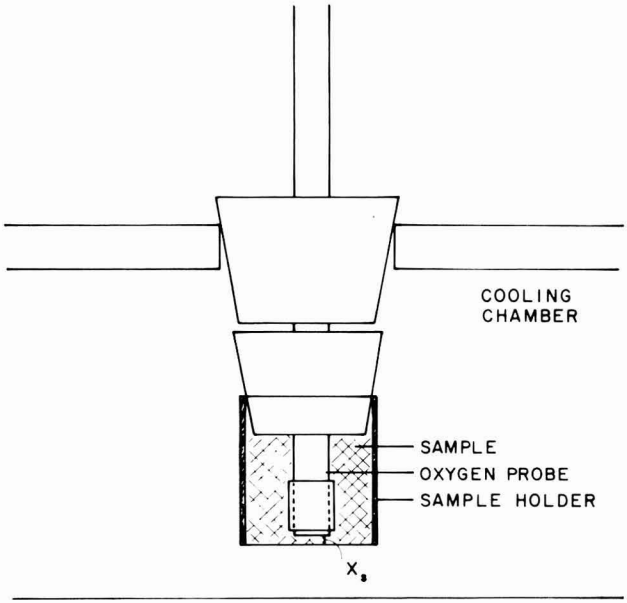

FIG. 2. SCHEMATIC DIAGRAM OF OXYGEN PROBE-SAMPLE CELL ASSEMBLY

All samples were maintained flat along the bottom of the copper jacket.

Slow frozen ice samples were prepared by stretching a small piece of polyethylene over the bottom of the copper jacket and filling the copper tube with water. The probe was lowered into the copper tube to obtain the desired thickness and the samples were then frozen in the controlled temperature chamber at $-5^{\circ}C$. The polyethylene film was removed after the samples were frozen.

Calcium alginate gels such as have been used to coat frozen fish were made by a two step film forming process. A 3.5% sodium alginate solution was poured into the copper cylinders with cheese cloth covering the bottom. The solution was quite viscous and did not leak. The probes were lowered to the desired depth, and then the entire probe assembly was placed in a 4.5% calcium lactate solution at room temperature. The calcium lactate which permeated through the cheese cloth caused crosslinking of the alginate in 2.5 days. Following removal from the calcium lactate solution, permeability readings were made on unfrozen gels at 5 and $0^{\circ}C$.

Minced fish samples were made by grinding fresh whole whiting. After being cleaned and filleted, the muscle was "minced" in a food grinder with 5 mm holes. At all times the fillets were kept on ice and

newly minced fish was kept refrigerated. It was noted that the minced whiting had a moisture content of 67% while the composition of filleted whiting was 77% water, 18% protein, and 3% fat. Thus, 10 g of distilled water were added for every 100 g of minced fish to approximate the moisture content of the whiting fillets. The minced fish had a consistency of a moist paste.

Minced fish was packed into the probe cell assembly and the surface smoothed in such a way that no visible gaps were present. Polyethylene was used to cover the samples until frozen. Again the effective sample thickness was varied by moving the probe tip relative to the open end of the holder. The packed density of slow frozen fish was 0.99 ± 0.06 g/cc. Sample permeability was measured at −5°C.

Oxygen Probe Operation

Probe to probe variation due to minor differences in construction and variation in permeability characteristics of individual membranes necessitated that each probe be individually calibrated and tested for linearity at −5°C using oxygen-nitrogen gas mixtures of different oxygen concentrations. An equilibration period of about two minutes was required during calibration. All diffusion analyses were based on steady state in which the probe response and presumably oxygen transport had reached equilibrium values. The probe's internal circuit was short-circuited when readings were not being taken, as this allowed oxygen to be continually consumed, holding internal oxygen concentration at 0%. While probe response was sufficiently constant over the 2 to 3 day period of a diffusion experiment, the probes were individually calibrated before and after each experiment at 0 and 20% oxygen to verify their constancy.

For the permeability tests rubber stoppers were used to hold the probe assembly with sample holder in a cooling chamber. The temperature of the chamber was controlled by a thermoelectric cooling element. Oxygen content of the atmosphere within the chamber was controlled by flushing the chamber with different nitrogen-oxygen gas mixtures.

Determination of Permeability Values

The Clark-type oxygen probe is used to measure the steady state oxygen concentration in the sample adjacent to the teflon membrane. The teflon membrane is permeable to oxygen, but not to liquids, and the probe is permeable to oxygen only at the membrane.

Oxygen diffusing through the membrane is immediately reduced at

the silver cathode directly behind the membrane so the oxygen concentration inside the probe is zero. Hydroxyl ions formed at the silver cathode migrate to the anode and combine with the lead ions. The net reaction is consumption of oxygen with production of lead hydroxide and the flow of electrons. The amount of current produced is limited by the diffusion of oxygen across the teflon membrane and can be expressed (assuming zero oxygen in the probe) by Fick's Law:

$$\frac{dO_2}{dt} = \frac{P_m (A)(p_{oe})}{X_m} \tag{1}$$

where

$\frac{dO_2}{dt}$ = rate of oxygen transport
P_m = permeability of teflon membrane
A = area of membrane available for flow
p_{oe} = pressure of oxygen external to probe
X_m = thickness of teflon membrane

The cell reaction (i.e. flow of electrons producing current) is directly related to the oxygen consumption and is expressed by

$$I = (n)(F)\frac{dO_2}{dt} \tag{2}$$

where

I = current produced (in amperes)
n = number of Faradays per mole of oxygen at electrode reaction
F = Faraday = 96,500 coulombs
$\frac{dO_2}{dt}$ = rate of oxygen transport (moles/s)

Combining Equations (1) and (2) gives

$$I = \frac{(n)(F)(P_m)(A)(p_{oe})}{X_m} \tag{3}$$

Thus it is seen that the performance of a probe is dependent on the membrane permeability, surface area permeable to oxygen, and thickness of the membrane; temperatures and oxygen partial pressure are external determinants of probe response. For any given probe at a

constant temperature, Equation (3) reduces to

$$I = K' p_{o\,e} \tag{4}$$

While the probes maintained a linear response to oxygen concentration, output current dropped with lowered temperature, due to decreased oxygen permeability of the membrane as temperature was reduced. A teflon permeability value of

$$\frac{337 \text{ cc-mil}}{100 \text{ in.}^2 \text{ day-atm}}$$

at $-5°C$ was obtained by extrapolation of teflon permeability data (DuPont Chemical Co. Technical Bulletin T-3B) (Fig. 3).

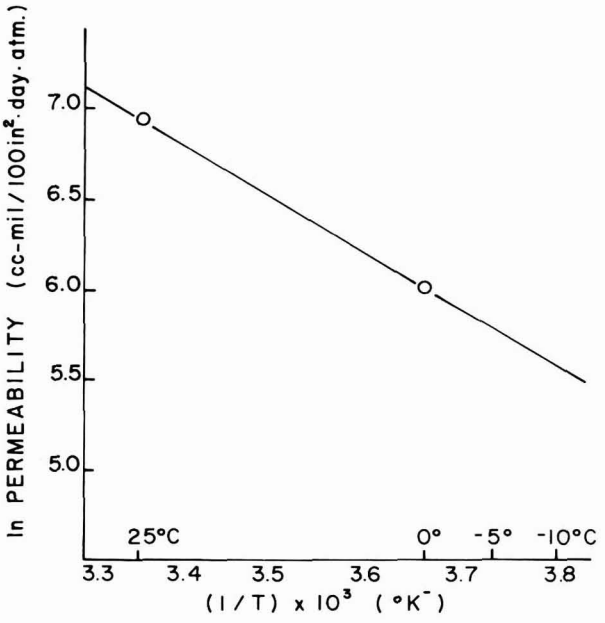

FIG. 3. PERMEABILITY OF TEFLON FILM TO OXYGEN

When a sample is placed on the probe, its resistance to oxygen flow is in series with the membrane resistance. This overall oxygen transport rate (which now determines the probe output) can be expressed by

$$\frac{dO_2}{dt} = P^*(A)(p_{oe}) \tag{5}$$

where P* is the overall permeability, which can be expressed as

$$P^* = \frac{1}{\frac{X_m}{P_m} + \frac{X_s}{P_s}} \tag{6}$$

in which X_s and P_s represent sample thickness and permeability, respectively. Now, combining Equations (2) and (5) gives

$$\frac{dO_2}{dt} = P^*(A)(p_{oe}) = \frac{I}{(n)(F)} \tag{7}$$

which upon rearranging becomes

$$P^* = \frac{I}{(n)(F)(p_{oe})(A)} \tag{8}$$

For a given probe, n, F, and A are constant; therefore

$$P^* = \frac{K''I}{p_{oe}} \tag{9}$$

Combining Equations (6) and (9) gives

$$\frac{K''I}{p_{oe}} = \frac{1}{\frac{X_m}{P_m} + \frac{X_s}{P_s}} \tag{10}$$

which rearranges to

$$\frac{1}{K''}\frac{p_{oe}}{I} = \frac{X_m}{P_m} + \frac{X_s}{P_s} \tag{11}$$

Now, by plotting p_{oe}/I versus X_s, the intercept is equal to K'' (X_m/P_m) and the slope = K'' $(1/P_s)$. By knowing (X_m/P_m), K'' can be determined. For experiments conducted at constant oxygen

concentration, 1/I can be plotted versus X_s, with the concentration factor included in K″. This method requires multiple thicknesses of the sample on one probe to determine a good straight line for the slope determination.

In cases where samples are evaluated at a single thickness, the permeability value can be determined by measuring the probe current of the base membrane (I_m) and of the membrane-sample combination (I_s). In this case Equation (11) can be expressed as

$$\frac{p_{oe}}{K''}\frac{1}{I_s} = \frac{p_{oe}}{K''}\frac{1}{I_m} + \frac{X_s}{P_s} \tag{12}$$

which can be rearranged to give

$$P_s = \frac{K''X_s}{p_{oe}\left[\dfrac{I_m - I_s}{(I_m)(I_s)}\right]} = \frac{K'''X_s}{\left[\dfrac{I_m - I_s}{(I_m)(I_s)}\right]} \tag{13}$$

In practice, the probe current readings have been normalized so that the bare probe membrane will read 0.00×10^{-6} amps when exposed to 0% oxygen, and 1.00×10^{-6} amps when exposed to air (20% oxygen) at the testing temperature. Probe readings with samples will therefore be between 0.00 and 1.00. Since all permeability tests were conducted at an oxygen partial pressure of 0.209 atm the use of normalized probe current means the term

$$K''' = \frac{K''}{p_{oe}} = \frac{P_m}{(X_m)(I_m)}$$

of Equation (13) varies only with test temperature (i.e. membrane permeability). It should be noted that sample permeability values are calculated in terms of the permeability value of the teflon membrane. The results are thus presented in the same units as were available for the teflon, namely, cc-mil/100 in.^{2} day atm. At times in the text, these units have been denoted by the term "PU," for "permeability units."

RESULTS AND DISCUSSION

The combined oxygen probe-sample assembly system gave a linear response of probe current as the oxygen partial pressure in the test

chamber was increased (Fig. 4). The probe response per unit of oxygen partial pressure is seen to be independent of the oxygen partial pressure level, indicating that the combined transport resistance for the ice sample and probe membrane in series is independent of external oxygen partial pressure. When these results were plotted as p_{oe}/I versus X_s (Fig. 5), a linear relationship with an intercept of $K'' X_m / P_m$ and a slope of K''/P_s was obtained. It can be seen that the permeability of the fast frozen ice sample was independent of oxygen partial pressure, since the slope of Fig. 5 was constant for the range of partial pressures tested.

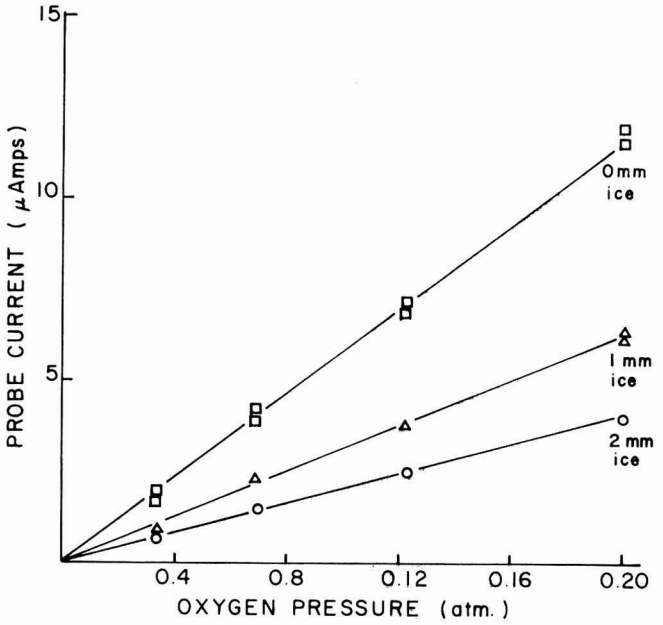

FIG. 4. DEPENDENCE OF OXYGEN PROBE CURRENT ON OXYGEN PARTIAL PRESSURE FOR THREE ICE THICKNESSES

The deviation of the data points from a straight line could indicate an incorrect measurement of sample thickness, changing permeability values as sample thickness increases, or both of these. For the data presented in Fig. 5, if the permeability value is assumed to be constant with thickness and the 0 and 2 mm ice thickness assumed correct, the deviation of the data points for the "1 mm thickness" would result from an error of thickness measurement of 0.1 mm. This indicates a need for careful measurement of thickness. If the thickness values are

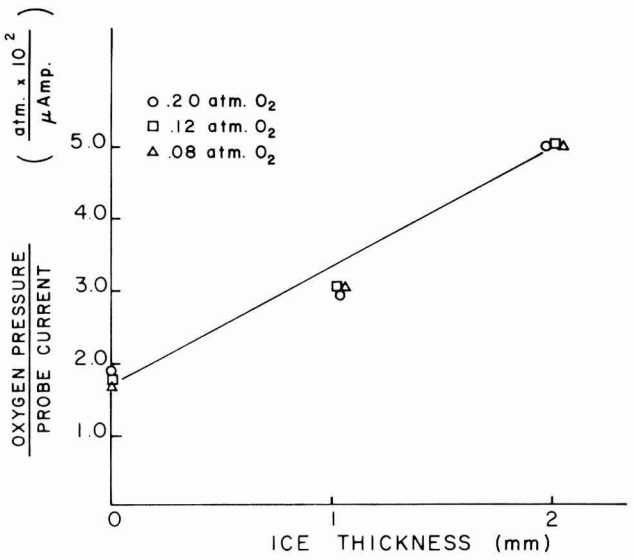

FIG. 5. DEPENDENCE OF OXYGEN PROBE CURRENT (NORMALIZED FOR OXYGEN PARTIAL PRESSURE) ON THICKNESS OF FAST FROZEN ICE

all assumed to be correct, then two permeability values can be calculated, one for each straight line segment. For the data of Fig. 5, these permeability values (in cc-mil/100 in.^{2} day atm) are 18,600 for the 1 mm thickness, and 11,600 for the 2 mm thickness, while the straight line assumption (i.e. the error is in thickness measurements) gave a value of 14,280. In most cases the average values for samples of measured thickness are given below.

Fast Frozen Ice

Measurements of the permeability of 2-mm thick fast frozen ice samples gave a range of values extending from 400 to 239,400 PU. Table 1 lists the individual values obtained. This wide variation of values indicates an inherent inhomogeneity of the ice structure for the different samples. During freezing, cracking sounds were heard and the ice crystals had visible imperfections. Although no quantitative correlation could be made between degree of cracking of the ice (as measured by the sound) and permeability, it can be speculated that imperfections due to cracks in the ice crystal allowed significantly increased oxygen transport. Fast frozen ice had a characteristic cloudy appearance which could be due to numerous small fractures throughout the ice. It was

Table 1. Permeability values for 2-mm thick fast frozen ice samples at −5°C (arbitrarily ordered by decreasing permeability values)

Sample Permeability in cc-mil / 100 in.^{2} day atm
239,400
59,200
45,300
33,900
32,500
26,600
19,300
13,700
13,100
13,100
7,500
4,000
3,300
960
400
400

also noted that when storing frozen samples, the fast frozen ice evaporated more rapidly than slow frozen ice, possibly due to the small fractures giving a larger specific surface area when exposed to the atmosphere.

Fast frozen thicker samples (up to 6 mm) had physical defects similar to those present in the thin samples, and thus while some 6 mm samples of fast frozen ice had no detectable oxygen transport, others had permeabilities up to 255,000 PU. Annealing the fast frozen ice tended to lower permeability, presumably by allowing the smaller cracks to fuse. However, in no case did annealing reduce the permeability to zero.

It was obvious that unambiguous permeability values for fast frozen ice were not possible, due to the inhomogeneities which existed from sample to sample. This information, nevertheless, indicates the fundamental variability that can be expected, and in particular it illustrates the potential difficulties which can result when applying ice glazes on samples at very low temperatures.

Slow Frozen Ice

For slow frozen ice at thicknesses of 2 mm or more, permeability to oxygen was undetectable with the probe system. Table 2 shows the range of values which were obtained for 1 mm thick slow frozen ice samples which were then locally melted to obtain samples of thicknesses of 0.4, 0.2, and 0.1 mm. Melting was repeated intermittently for 10 seconds and the samples then re-equilibrated at −5°C. This was done in order to keep the bulk of the sample at −5°C and restrict melting to the surface. After each melting a new permeability measurement was taken. The range of values within each thickness grouping is much closer than for fast frozen ice. (Values with asterisks were eliminated in the corrected average because their high values appeared to be due to imperfections such as air bubbles in the ice surface, which were not considered to be representative of the inherent structure of slow frozen

Table 2. Oxygen permeability values of slow frozen ice samples of various thickness at −5°C

Ice Thickness (mm)	Permeability Value	$\left[\frac{\text{cc-mil}}{100\ \text{in.}^2\ \text{day atm}}\right]$
1	NM[a]	
1	NM	
1	NM	
1	NM	
1	NM	
1	420	Average = 70
0.4	NM	
0.4	NM	
0.4	530	
0.4	800	
0.4	880	
0.4	3450[b]	Average = 440
0.2	200	
0.2	300	
0.2	300	
0.2	440	
0.2	950	
0.2	1510[b]	Average = 440
0.1	100	
0.1	120	
0.1	130	
0.1	150	
0.1	340	
0.1	2020[b]	Average = 170

[a]Not measurable
[b]Omitted from calculation of average permeability value

ice). Annealing slow frozen ice samples with high permeabilities by briefly raising the temperature of the ice surface resulted in new permeabilities comparable to other samples in the same thickness range. The probe output in series with slow frozen ice is fairly consistent in the thicknesses between 0.0 mm and 0.4 mm, which probably indicates some annealing of the sample in the "melting" process as well as some aspects of structure of thin samples of slow frozen ice.

To explain the limited oxygen permeability of slow frozen ice at thicknesses greater than 1 mm and the increased oxygen permeabilities at smaller thicknesses, it can be considered that slow frozen ice has

some limited number of small cracks or imperfections, each of which is presumably less than about 0.5 mm in length. In thicker samples these imperfections are not in communication and thus there is little or no oxygen transport through the whole sample. As sample thickness decreases, more and more "passages" for oxygen traverse the sample, and permeability increases. As noted above, the fact that the permeability shows its highest value (440 PU) at a thickness of about 0.2–0.4 mm for slow frozen ice, probably indicates that some annealing takes place when preparing the 0.1 mm samples.

Calcium Alginate Films

Table 3 shows that the permeability of various thicknesses of calcium alginate gels fell into two distinct groups which appear related to maintenance of structural integrity of the gel at 0°C. At 5°C all gels had similar permeability values. In 4 of the 7 gels, permeability decreased with decreasing temperature, with the average permeability at 0°C being 1230 PU. For the second group, the oxygen permeabilities increased strongly when held at 0°C, averaging 11,700 PU.

Table 3. Oxygen permeability of calcium alginate gels at 5 and 0°C

Gel Thickness (mm)	Permeability $\left(\frac{\text{cc-mil}}{100\ \text{in.}^2\ \text{day atm}}\right)$ (5°C)	(0°C)
	Samples with Decreasing Permeability	
1.2	2990	1980
1.2	4250	710
2.0	1040	610
3.2	7380	1610
	3915[a]	1230
	Samples with Increasing Permeability	
1.7	3430	4080
2.5	1960	20,800
3.0	—	10,100
	2700[a]	11,700

[a]Overall average for 6 samples at 5°C, 3510 ± 2200

The high permeability of the second set of samples is presumably due to ruptures in the gel structure, since crosslinking was conducted at room temperature and the set gels would contract when refrigerated. While generally causing a firming of the gel, this contraction could also produce stresses in the crosslinking structure, which might lead to ruptures. No large tears were evident in any gels on visual observation with the naked eye.

Slow Frozen Minced Fish

Table 4 shows the range of values which were obtained upon measuring the permeability of slow frozen minced fish flesh at −5°C. Each sample was independently prepared. The average oxygen permeability for each thickness was dependent on sample thickness, which suggests that oxygen is being transported through a non-homogeneous substance which varies in its resistance. As the sample gets thicker, areas of greater resistance are found in series with more porous areas, and the pathways of oxygen transport become "plugged." The dispersion of permeability values within the same thickness also indicates the nonuniform characteristics of the permeability of frozen minced fish flesh. It was noted that at a thickness of greater than 5 mm, virtually no diffusion was measured.

Water absorbed at the surface of the minced fish, such as with ice glazes, is expected to reduce oxygen permeability. Table 5 shows the effect of surface absorption of water on the permeability values measured at a depth of 1 mm in the minced fish. The first treatment consisted of dipping the fish-cell assembly into ice water and equilibrating at −5°C. The second dipping gave a complete water film on the fish surface, though there was no measurable increase in thickness of the sample. It is unlikely that any significant thawing of the fish tissue itself occurred in the short dipping time. In every case the oxygen permeability of fish decreased with the water coating treatment, while average permeability values decreased from 2323 PU (untreated) to 1565 PU. This is still significantly higher than an identical thickness of ice.

The effect of drying of the fish surface on permeability was evaluated by passing the air through a dessicant before it entered the cooling chamber, thus drying the exposed fish samples. At the end of the test period (24 h) the outer surfaces of the minced fish flesh were dry and very hard, and had contracted somewhat. The dryness was localized at the surface, with the underlying minced fish having a normal texture and moisture content.

Table 6 gives the average permeability values for seven 2 mm thick fish samples held in the dry air at −5°C for a 24-h period. Permeability

Table 4. Oxygen permeability values for slow frozen minced fish at −5°C

Sample Thickness (mm)	Permeability $\left(\frac{\text{cc-mil}}{100\ \text{in.}^2\ \text{day atm}}\right)$
2	2960
	2540
	1660
	580
	470
	250
	250
	1240
1	7010
	3020
	2340
	1450
	1240
	420
	400
	2270

Table 5. Effect of ice glazing on oxygen permeability of 1 mm thick minced fish at −5°C

Treatment	Permeability[a] $\left(\frac{\text{cc-mil}}{100\ \text{in.}^2\ \text{day atm}}\right)$
Frozen minced fish	2320
Frozen minced fish with quick dip	1860
Frozen minced fish with "complete" layer of ice	1570

[a]Average of 7 values

decreased from an initial value of 920 to 327 PU after 24 h of drying. The structural changes associated with freezer burn apparently increase the resistance of minced fish to oxygen transport. Of course, freezer

Table 6. Effect of surface dessication on oxygen permeability of frozen minced fish at −5°C

Exposure Time to Cold Dry Air (h)	Permeability[a] $\left(\frac{\text{cc-mil}}{100\ \text{in.}^2\ \text{day atm}}\right)$
0	920
2.5	920
5	640
9.5	490
11.5	440
20	410
24	330

[a]Average of 7 values

burn does cause significant problems with respect to storage quality of food products, and would not be a recommended method to reduce oxygen diffusion.

SUMMARY

Lipid oxidation within a frozen minced fish sample will be affected by both incorporation of oxygen in the sample and transport of oxygen through the sample. It has been shown that oxygen can permeate through minced fish and through materials such as ice and calcium alginate gel, which are often used to coat frozen fish products.

Fast frozen ice samples showed widely ranging values of oxygen permeability, even at thickness of 6 mm. Slow frozen ice had much lower permeability values, and at thicknesses above 2 mm was essentially impermeable. Calcium alginate gel samples could be divided into 2 groups, based on if oxygen permeability increased or decreased as the temperature was lowered from 5 to 0°C. Slowly frozen minced fish was somewhat more permeable to oxygen than an equal thickness of slow frozen ice. Surface dessication or application of an ice glaze reduced oxygen permeability of the frozen minced fish.

It is proposed that oxygen transport occurs mainly through physical defects in the frozen material, such as cracks or holes. The high transport rates in fast frozen ice would reflect the significant sounds heard during freezing. Annealing processes, which would give repair of some physical defects, were found to reduce the oxygen transport in ice samples. The behavior of the calcium alginate gel samples can also be

explained on the basis of physical defects in the matrix resulting from contraction stresses arising during the cooling of the crosslinked samples. With the minced fish samples, besides the presence of physical defects, there could also be some influence of "unfrozen" water in the fish, as the test temperature was only −5°C.

ACKNOWLEDGMENT

This project was supported by Contract No. 03-5-043-319 from the National Marine Fisheries Service, U.S. Department of Commerce.

REFERENCES

ADAMSON, A. W., DORMANT, L. M. and OREM, M. 1967. Physical adsorption of vapors on ice 1. Nitrogen. J. Coll. Interf. Sci. *25*, 206–217.

ADAMSON, A. W. and JONES, B. R. 1971. Physical adsorption of vapors on ice IV. Carbon dioxide. J. Coll. Interf. Sci. *37*, 831–835.

ANDERSSON, L. and DANIELSON, C. E. 1961. Storage changes in frozen fish. A comparison of objective and subjective tests. Food Technol. *15*, 55–57.

BAUERNFEIND, J. C. 1953. Use of ascorbic acid in processing foods. Adv. Food Res. *4*, 356–431.

CHARM, S. E. and MOODY, P. 1966. Bound water in haddock muscle. ASHRAE J. *8*(4), 39–42.

DINGLE, J. R. and HINES, J. A. 1975. Protein instability in minced flesh from fillets and frames of several commercial Atlantic fishes during storage at −5°C. J. Fish. Res. Bd. Canada *32*, 775–783.

DUCKWORTH, R. B. 1971. Differential thermal analysis of frozen food systems. I. The determination of unfreezable water. J. Food Technol. *6*, 317–327.

EL-SHERBIENY, A. M. 1969. The porosity of frozen tissue, solution and/or ice. In *Progress in Refrigeration Science and Technology*, pp. 1063–1069, Proceeding of the 12th International Congress of Refrigeration, Madrid, 1967, International Institute of Refrigeration.

GLICKSMAN, M. 1969. Seaweed extracts: Alginates. In *Gum Technology in the Food Industry*, Chap. 8, Academic Press, New York.

JELLINEK, H. H. G. 1967. Liquid-like (transition) layer on ice. J. Coll. Interf. Sci. *25*, 192–205.

JOHNSON, M. J., BORKOWSKI, J. and ENGBLOM, C. 1964. Steam sterilizable probes for dissolved oxygen measurements. Biotech. Bioeng. *7*, 457–468.

KAREL, M. 1975. Physico-chemical modification of the state of water in foods—A speculative survey. In *Water Relations of Foods*, (R. B. Duckworth, ed.), pp. 435–463, Academic Press, London.

KENT, M. 1975. Fish muscle in the frozen state: Time dependence of its microwave dielectric properties. J. Food Technol. *10*, 91–102.

LAMBERT, D., FLINK, J. and KAREL, M. 1973a. Volatile transport in frozen aqueous solutions. I. Development of a mechanism. Cryobiology *10*, 45–51.

LAMBERT, D., FLINK, J. and KAREL, M. 1973b. Volatile transport in frozen

aqueous solutions. II. Influence of system parameters. Cryobiology *10*, 52–55.
MIYAUCHI, D., PATASHNIK, M. and KUDO, G. 1975. Frozen storage keeping quality of minced black rockfish (Sebastes spp.) improved by cold-water washing and use of fish binder. J. Food Sci. *40*, 592–594.
OLCOTT, H. S. 1962. Marine products. In *Lipids and Their Oxidation*, (H. W. Schultz, E. A. Day and T. R. O. Sinnhuber, eds.), Chap. 6, Avi Publishing Co., Westport, Conn.
REIHL, N., STACHELEN, P. and HAHNE, E. 1973. In *Physics and Chemistry of Ice*, E. Whalley, J. J. Jones and L. W. Gould, eds.), pp. 170–172, Royal Society of Canada, Ottawa.
STOREY, R. M. 1970. The diffusion of water in frozen cod. In *Supplement to the Bull. Intern. Inst. of Refrig.*, Leningrad Intern. Inst. of Refrigeration.
TAPPEL, A. L. 1962. Hematin compounds and lipoxidase as biocatalysts. In *Lipids and Their Oxidation*, (H. W. Schultz, E. A. Day and T. R. O. Sinnhuber, eds.), Chap. 6, Avi Publishing Co., Westport, Conn.
TARR, H. L. A. 1947. Control of rancidity in fish flesh. I. Chemical antioxidants. J. Fish. Res. Bd. Canada *7*, 137–154.
TARR, H. L. A. 1948. Control of rancidity in fish flesh. II. Physical and chemical methods. J. Fish. Res. Bd. Canada *7*, 237–247.

F
N
P

JOURNALS AND BOOKS IN FOOD SCIENCE AND TECHNOLOGY

JOURNAL OF FOOD BIOCHEMISTRY — Herbert O. Hultin
Norman F. Haard and John R. Whitaker

JOURNAL OF FOOD PROCESS ENGINEERING —
Dennis R. Heldman

JOURNAL OF FOOD PROCESSING AND PRESERVATION —
Theodore P. Labuza

JOURNAL OF FOOD QUALITY — Amihud Kramer and
Mario P. DeFigueiredo

JOURNAL OF FOOD SAFETY — M. Solberg and Joseph D. Rosen

JOURNAL OF TEXTURE STUDIES — P. Sherman and
Alina S. Szczesniak

FOOD POISONING AND FOOD HYGIENE, FOURTH EDITION —
Betty C. Hobbs and Richard J. Gilbert

FOOD SCIENCE AND TECHNOLOGY, THIRD EDITION —
Magnus Pyke

POSTHARVEST BIOLOGY AND BIOTECHNOLOGY —
Herbert O. Hultin and Max Milner

PRINCIPLES OF FOOD SCIENCE — Georg Borgstrom
VOLUME 1 — FOOD TECHNOLOGY
VOLUME 2 — FOOD MICROBIOLOGY AND BIOCHEMISTRY

THE SCIENCE OF MEAT AND MEAT PRODUCTS,
SECOND EDITION —
James F. Price and B. S. Schweigert

GUIDE FOR AUTHORS

Typewritten manuscripts in triplicate should be submitted to the editorial office. The typing should be double-spaced throughout with one-inch margins on all sides.

Page one should contain: the title, which should be concise and informative; the complete name(s) of the author(s); affiliation of the author(s); a running title of 40 characters or less; and the name and mail address to whom correspondence should be sent.

Page two should contain an abstract of not more than 150 words. This abstract should be intelligible by itself.

The main text should begin on page three and will ordinarily have the following arrangement:

Introduction: This should be brief and state the reason for the work in relation to the field. It should indicate what new contribution is made by the work described.

Materials and Methods: Enough information should be provided to allow other investigators to repeat the work. Avoid repeating the details of procedures which have already been published elsewhere.

Results: The results should be presented as concisely as possible. Do not use tables *and* figures for presentation of the same data.

Discussion: The discussion section should be used for the interpretation of results. The results should not be repeated.

In some cases it might be desirable to combine results and discussion sections.

References: References should be given in the text by the surname of the authors and the year. *Et al.* should be used in the text when there are more than two authors. All authors should be given in the References section. In the Reference section the references should be listed alphabetically. See below for style to be used.

DEWALD, B., DULANEY, J. T. and TOUSTER, O. 1974. Solubilization and polyacrylamide gel electrophoresis of membrane enzymes with detergents. In *Methods in Enzymology*, Vol. xxxii, (S. Fleischer and L. Packer, eds.) pp. 82–91, Academic Press, New York.

HASSON, E. P. and LATIES, G. G. 1976. Separation and characterization of potato lipid acylhydrolases. Plant Physiol. *57*, 142–147.

ZABORSKY, O. 1973. *Immobilized Enzymes*, pp. 28–46, CRC Press, Cleveland, Ohio.

Journal abbreviations should follow those used in *Chemical Abstracts*. Responsibility for the accuracy of citations rests entirely with the author(s). References to papers in press should indicate the name of the journal and should only be used for papers that have been accepted for publication. Submitted papers should be referred to by such terms as "unpublished observations" or "private communication." However, these last should be used only when absolutely necessary.

Tables should be numbered consecutively with Arabic numerals. The title of the table should appear as below:

Table 1. Activity of potato acyl-hydrolases on neutral lipids, galactolipids, and phospholipids

Description of experimental work or explanation of symbols should go below the table proper.

Figures should be listed in order in the text using Arabic numbers. Figure legends should be typed on a separate page. Figures and tables should be intelligible without reference to the text. Authors should indicate where the tables and figures should be placed in the text. Photographs must be supplied as glossy black and white prints. Line diagrams should be drawn with black waterproof ink on white paper or board. The lettering should be of such a size that it is easily legible after reduction. Each diagram and photograph should be clearly labeled on the reverse side with the name(s) of author(s), and title of paper. When not obvious, each photograph and diagram should be labeled on the back to show the top of the photograph or diagram.

Acknowledgments: Acknowledgments should be listed on a separate page.

Short notes will be published where the information is deemed sufficiently important to warrant rapid publication. The format for short papers may be similar to that for regular papers but more concisely written. Short notes may be of a less general nature and written principally for specialists in the particular area with which the manuscript is dealing. Manuscripts which do not meet the requirement of importance and necessity for rapid publication will, after notification of the author(s), be treated as regular papers. Regular papers may be very short.

Standard nomenclature as used in the scientific literature should be followed. Avoid laboratory jargon. If abbreviations or trade names are used, define the material or compound the first time that it is mentioned.

EDITORIAL OFFICE: Prof. T. P. Labuza, Editor, Journal of Food Processing and Preservation, University of Minnesota, Department of Food Science and Nutrition, Saint Paul, Minnesota 55108 USA

JOURNAL OF FOOD PROCESSING & PRESERVATION Vol. 2, No. 3

CONTENTS